



OPEN

Aminothioliol supported dialdehyde cellulose for efficient and selective removal of Hg(II) from aquatic solutions

Aya G. Mostafa, Eslam A. Gaith & Magda A. Akl

The increasingly serious problem of mercury pollution has caused wide concern, and exploring adsorbent materials with high adsorption capacity is a simple and effective approach to address this concern. In the recent study, dialdehyde cellulose (DAC), cyanoacetohydrazide (CAH), and carbon disulfide (CS₂) are used as raw materials for the (DAC@CAH@SK₂) preparation material through the three-steps method. By utilizing the following characterization techniques; thermogravimetric analysis (TGA), N₂ adsorption–desorption isotherm (BET), elemental analysis, scanning electron microscopy (SEM), Fourier transform infrared spectroscopy (FTIR), and X-ray diffraction (XRD), ¹HNMR and Energy Dispersive X-ray Spectroscopy (EDS) of DAC@CAH@SK₂ composite. The point of zero charge (pH_{PZC}) for the prepared DAC@CAH@SK₂ also was examined. From the batch experiments, the optimum conditions were found to be pH (5–8), an Hg²⁺ concentration of 150 mg/L, a DAC@CAH@SK₂ dose of 0.01 g, and a contact time of 180 min with a maximum adsorption quantity of 139.6 mg/g. The process of Hg²⁺ adsorption on the DAC@CAH@SK₂ material was spontaneous exothermic, monolayer chemisorption, and well-fitted to Langmuir and pseudo-2nd-order models. The DAC@CAH@SK₂ selectivity towards the Hg²⁺ was examined by investigating the interfering metal ions effect. The DAC@CAH@SK₂ was successfully applied for the Hg²⁺ removal from synthetic effluents and real wastewater samples with a recovery % exceeding 95%. The prepared DAC@CAH@SK₂ was regenerated using a mixture of EDTA and thiourea. Also, FT-IR analysis indicates that the synergistic complexation of N and S atoms on DAC@CAH@SK₂ with Hg(II) is an essential factor leading to the high adsorption capacity.

The rapid growth of industry, population, and urbanization causes significant water contamination^{1,2}. Mercury(II) is considered an extremely toxic contaminant that can easily accumulate in the human body³. It poses a dangerous threat to the environment and living organisms' health as it causes such serious illnesses as paralysis, birth defects, mental disorders, and other hazardous diseases. Additionally, methanogens and other bacteria can convert inorganic mercury into a more toxic form, organic mercury, which mainly causes severe harm to human nerves and the brain^{4–6}. Due to the risk of chronic poisoning, the Joint Food and Agriculture Organization and the World Health Organization (FAO/WHO) recommend that total mercury intake not exceed 5 µg/kg body weight per week, and the maximum permitted mercury concentration in drinking water is 30 nM^{2,7,8}. Natural water bodies' contamination by Hg(II) mainly comes from dyes, batteries, mining, and pulp industries^{9,10}.

In response to the problem of water contamination by the Hg(II) ions, many techniques have been employed to solve it¹¹, such as bioremediation¹², membrane filtration¹³, photocatalytic degradation¹⁴, electrochemical techniques¹⁵, ion exchange¹⁶, and adsorption¹⁷. Adsorption is seen to be a more desirable technique for toxic heavy metals removal from the contaminated water than the other mentioned methods due to its simplicity, high efficiency, cheapness, and ability to handle large-scale systems¹⁸. Consequently, effective adsorbent development is an essential issue in the adsorption process¹⁹. Many materials have been utilized as adsorbents like chitosan²⁰, activated carbon²¹, clay²², cellulose-based materials²³, nanosized metal oxides²⁴, and metal–organic frameworks²⁵.

Cellulose is a naturally occurring polymer that has various advantages as it is considered cost-effective, available, reusable, and environmentally friendly material. It can be derived from many natural sources, like cotton, bamboo, and straw. It has a relatively low adsorption efficiency because of its lack of functional groups. In order

Department of Chemistry, Faculty of Science, Mansoura University, Mansoura 35516, Egypt. email: magdaakl@yahoo.com

to increase the adsorption efficiency, the cellulose chemical modification is occurred by introducing new desired functional groups. Cellulose has an abundance of hydroxyl groups that can be chemically modified by esterification, grafting, oxidation, or etherification, in order to prepare highly efficient cellulose-based adsorbents^{26–30}. When compared to unmodified cellulose, modified cellulose had higher efficiency for adsorbing heavy metal ions³¹. Cellulose that had been treated with a sulfo group had greater adsorption efficiency³².

Cellulose-based adsorbents have been reported for various contaminants remediation such as arsenic³³, Cr(IV)³⁴, (Hg(II), Cd(II), Cu(II), and Pb(II))³⁵, uranium (VI)³⁶, and Cu(II)³⁷. Moreover, dialdehyde cellulose microfibers have been utilized for the removal of eriochrome black T dye³⁸. The removal of Cu²⁺, Hg²⁺, and Pb²⁺ was investigated using guanyl thiosemicarbazide functionalized dialdehyde cellulose³⁹. Recently, Akl et al. used a semicarbazide modified Flax fiber biomaterial for the Cr(VI) and Alizarin Red S anionic dye removal⁴⁰.

Here, cellulose adsorption capability enhancement was obtained by the modification of it with cyanoacetohydrazide and CS₂ in the presence of KOH in order to obtain adsorbent (DAC@CAH@SK₂) rich with nitrogen and sulfur functional groups that acts as a chelating agent. Correspondingly, the effectiveness of the DAC@CAH@SK₂ material in Hg²⁺ adsorption from aqueous solutions and various real water samples was investigated. Adsorbents modification by ligands containing sulfur, nitrogen, and oxygen functional groups have shown high binding affinity toward Hg(II) ions. Current research has focused on the development of adsorbents with sulfur/Nitrogen-based as these functional groups are well known for Hg(II) remediation efficiency enhancement through soft Lewis's acid-based interaction. The multifunctional nature of DAC@CAH@SK₂ is expected to enhance Hg(II) adsorption capacity^{39–46}. As of now, very little work has been reported on the use of DAC@CAH@SK₂ for the removal of Hg(II) ions from aquatic solutions.

According to our knowledge, cellulose modification using a nitrogen-containing ligand (cyanoacetohydrazide) and a Carbon disulfide has not been reported in the literature. Furthermore, no data were found on utilizing DAC@CAH@SK₂ modified cellulose as an effective adsorbent/chelating agent for Hg²⁺ removal from actual polluted water samples.

Accordingly, the following goals guided the performance of the current study:

1. Design and synthesis of DAC@CAH@SK₂ composite for adsorption of Hg²⁺ in aqueous solutions.
2. Characterization of the as-prepared DAC@CAH@SK₂ composite utilizing physical (optical images), elemental analysis (CHNS), and spectroscopic (FTIR), SEM, ¹HNMR and EDS, XRD, BET, and TGA instrumental performances.
3. Batch experiments of Hg²⁺ pollutant adsorption.
4. Investigating the optimum parameters required for optimal adsorption of the Hg²⁺, e.g., pH, temperature, the initial Hg²⁺ concentration, the mass of DAC@CAH@SK₂ composite, and the oscillation time, ionic strength as well as the interfering ions.
5. Studying the various adsorption isotherm, kinetics, and thermodynamic parameters.
6. Hg²⁺ removal efficiency and reusability of DAC@CAH@SK₂ composite comparison with other previously reported adsorbents.
7. Clarification of the mechanism involved in the process of Hg²⁺ adsorption onto DAC@CAH@SK₂ composite.

Experimental Materials

Cellulose powder, cyanoacetohydrazide, Carbon disulfide, hydrogen disulfide, potassium periodate (KIO₄), potassium hydroxide (KOH), mercury chloride (HgCl₂), HCl, NaOH, glacial acetic acid, ethanol, and NaCl were bought from Sigma Aldrich. A 4% potassium periodate solution was prepared by liquefy 4 g of KIO₄ in 100 ml dist.H₂O.

Instrumentation

The p*H*_{PZC} of DAC@CAH@SK₂ was estimated as follows: 100mg of the DAC@CAH@SK₂ chelating agent was added to a 25 ml 0.01M NaCl pH-adjusted solutions (2–12) and then the mixtures were shaken at the equilibrated shaker for 48 h. NaCl pH adjustment occurred by 0.1 M of HCl and 0.1 M of NaOH. The final pH was recorded after the shaking and ΔpH was calculated as in the following Eq (ΔpH = p*H*_f – p*H*_i). In order to obtain the p*H*_{PZC} value, ΔpH was plotted against the initial pH (p*H*_i). As the p*H*_{PZC} value, ΔpH = 0, is the point where X-axis (ΔpH) crosses the ΔpH vs p*H*_i curve^{47,48}.

Fourier transform infrared, FTIR, spectra of DAC, DAC@CAH, DAC@CAH@SK₂ composite, the DAC@CAH@SK₂-Hg²⁺, as well as the native cellulose were obtained at wavenumber range (4000–400 cm⁻¹) by a Perkin-Elmer, Spectrum RX I using KBr pellets. The DAC, DAC@CAH, DAC@CAH@SK₂, and DAC@CAH@SK₂-Hg²⁺ surface morphologies were examined by scanning electron microscopy (A JSM-6510LV) that was used, also, to obtain the EDS (Energy Dispersive X-ray Spectroscopy) spectral investigation of the DAC@CAH@SK₂-Hg²⁺. A PAN analytical X'Pert PRO diffractometer was employed for the X-ray diffraction (XRD) patterns of the DAC, DAC@CAH@SK₂, and DAC@CAH@SK₂-Hg²⁺ samples investigation at (4–70°) range of 2-theta (θ). The native cellulose, DAC@CAH, and DAC@CAH@SK₂ materials specific surface area (S_{BET}) was investigated utilizing the Brunauer Emmet Teller (BET) analysis (Size Analyzer (QUANTACHROME—NOVA 2000 Series)). The CHNS composition determination of native cellulose, DAC@CAH, and DAC@CAH@SK₂ was obtained by a Costech ECS-4010 elemental analyzer. The thermal stability of DAC@CAH@SK₂ and DAC@CAH@SK₂-Hg²⁺ materials was examined by thermogravimetric analysis (Berkin Elmer TGA 4000) at a heating rate of 15 °C/min from 30 to 800 °C. The ¹HNMR spectra of the prepared DAC and DAC@CAH@SK₂ materials were measured in a mixture of DMSO/trifluoroacetic acid (TFA) using a Joel 500 MHZ Japan.

Preparations

preparation of dialdehyde cellulose (DAC) and the aldehyde content (%) estimation

In the complete absence of light, the cellulose (one gram) oxidation occurred using 4% KIO_4 (100 ml), as present in Fig. 1. The previous mixture was shaken for 6 h. The obtained oxidized cellulose (DAC) was washed by dist. H_2O followed by the DAC drying step in an oven at 50°C ³⁹. The aldehyde content (AC %) of the prepared DAC was determined as reported previously^{39,40}, 0.1 g of the prepared DAC was added to 25 mL of 250 mM pH 4 adjusted hydroxylamine HCl then the mixture was stirred at room temperature in complete darkness for 2.5 h. Then, DAC was filtered and dried in an oven for 60 min at 70°C . The filtrate was back-titrated utilizing 0.1 M NaOH to pH 4 and the reaction endpoint was achieved when the color shifted from red to yellow. The control experiment was performed by replacing the DAC with native material. The estimation of the prepared DAC aldehyde content percentage (AC (%)) has occurred using Eq. (1).

$$\text{AC \%} = \frac{\text{NaOH Concentration} (V_{\text{sample}} - V_{\text{control}})}{m/\text{Mwt}} \quad (1)$$

Where V_{sample} and V_{control} are the volumes of NaOH in the case of oxidized cellulose and native cellulose powder, respectively. While m is sample weight and Mwt is cellulose molecular weight.

Preparation of cyanoacetohydrazide/carbon disulfide modified dialdehyde cellulose (DAC@CAH@SK₂) sorbent

At first, 4 g of cyanoacetohydrazide were dissolved in ethanol and were added to 1.5 g of DAC with the addition of 2 drops of glacial acetic acid. The previous mixture was allowed to reflux for 6 h at 70°C to form DAC@CAH material. Then the mixture was filtered and washed with ethanol. After drying the DAC@CAH material at 45°C , it was added to 10ml CS_2 then 40 ml of ethanol was added. The mixture was stirred for 8 h at room temperature. Then 1ml of KOH solution was added to the previous mixture and allowed to stir for 15 min at room temperature. Finally, the mixture was filtered and the obtained DAC@CAH@SK₂ material was washed with ethanol and dist. H_2O and dried in an oven at 45°C . The subsequent steps of preparation of DAC@CAH@SK₂ are illustrated in Fig. 2.

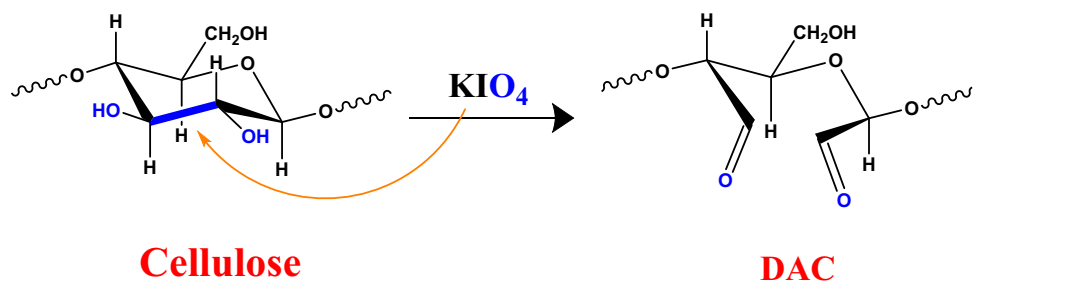


Figure 1. Preparation of 2,3 dialdehyde cellulose (DAC).

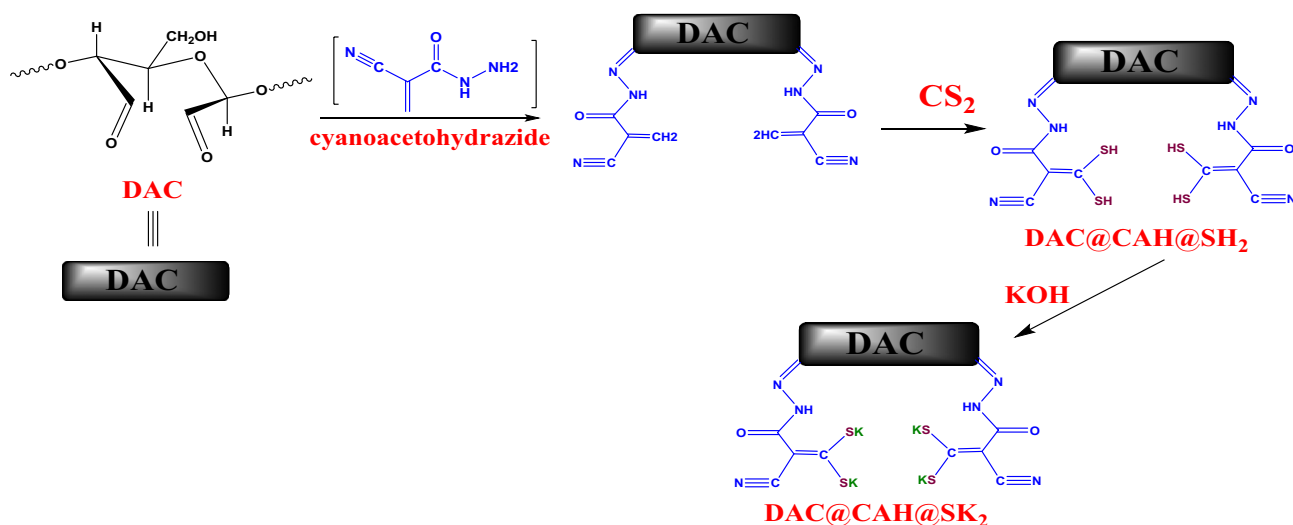


Figure 2. Synthesis of DAC@CAH@SK₂.

Adsorption and regeneration experiments

Batch adsorption

The adsorption behavior of Hg^{2+} using the DAC@CAH@SK₂ material was investigated through batch adsorption experiments in 50 ml stoppered bottles that contained 10 mL of Hg^{2+} solutions and DAC@CAH@SK₂ dose. Various parameters were investigated including pH (from 1 to 10), metal ion concentration (25–400 mg/L), chelating agent weight (0.001–0.015 g), and oscillation time (30–300 min). Unless specified otherwise, the pH, DAC@CAH@SK₂ dose, concentration, and contact time were fixed to 6.0, 0.01 g, 150 ppm, and 3.0 h, respectively. The pH was adjusted using diluted HCl and NaOH solutions. The concentration of Hg^{2+} upon each adsorption experiment was determined by ICP-OES (Agilent's 5100 instrument). The removal (%) and adsorption capacity at equilibrium (q_e) was determined using Eqs. (2) and (3), respectively⁴⁷.

$$R\% = \frac{C_i - C_f}{C_i} \times 100 \quad (2)$$

$$q_e = \frac{(C_i - C_f) \times V}{m} \quad (3)$$

C_i and C_f are the initial and equilibrium Hg^{2+} concentration (ppm), respectively. While m (g) is the DAC@CAH@SK₂ dose and V (L) is the adsorbate solution volume.

Desorption and regeneration

Regeneration of DAC@CAH@SK₂ composite was obtained through 5 adsorption–desorption following cycles. Hg(II) adsorption experiments were carried out by utilizing 0.01 g of DAC@CAH@SK₂ and 10 mL (150 mg/L) of Hg(II) solution at pH 7 for 2 h. For desorption investigation, 10 ml of HNO₃ 0.1M- thiourea 0.1M mixture (1:1) and 0.01 g of DAC@CAH@SK₂- Hg^{2+} were shaken for 2 h⁴⁹. Finally, the regenerated DAC@CAH@SK₂ chelating agent was reused for another five repeated adsorption–desorption cycles.

Adsorption Selectivity

A total of 10 mg of DAC@CAH@SK₂ composite was added to a 10 ml solution of binary metal ions and multiple metal ions synthetic mixtures (with the same concentrations of each metal ion (150 mg L⁻¹)) and shaken at 25 °C for 2 h. The added metal ions concentrations were estimated by ICP OES and the adsorption capacities were calculated with Eq. (3), and then the adsorption selective coefficient (α) was defined as presented in Eq. (4):

$$\alpha = \frac{\text{The adsorption capacity of Hg (II) on DAC@CAH@SK}_2}{\text{The adsorption capacity of coexisting metal ion on DAC@CAH@SK}_2} \quad (4)$$

Application

150 mg/L of Hg^{2+} was spiked to the real (sea, waste, and tap) water samples. Before the spiking step, the real water samples were digested by adding a mix of K₂S₂O₈ (0.5 g) and H₂SO₄ (5 ml, 98% (w/w)) to 1000 ml of each water sample and then heated for 120 min at 90 °C for complete digestion of presented organic materials. After cooling to room temperature, 0.01 g of DAC@CAH@SK₂ was added to the prepared samples, and the pH value was adjusted to 7 with continuous shaking for 180 min. The solutions were centrifuged and again another 0.01 g of DAC@CAH@SK₂ was added to the supernatant to ensure the complete separation of analytes. The remaining Hg^{2+} was determined using ICP OES.

Results and discussion

Materials' design

DAC synthesis

The KIO₄ oxidizing agent is a known selective one that is utilized for the oxidation of two OH groups that are present on the glucopyranoside ring's C₂–C₃ neighboring carbon atoms. KIO₄ cleaves the bond between C₂–C₃ and the OH groups are converted into two dialdehyde groups. The oxidation degree which represents the percentage of monosaccharide units that reacted with KIO₄ is calculated by aldehyde content determination³⁹. The AC % of the synthesized DAC is 38.93% as shown in Table 1.

V _{control} (ml)	V _{sample} (ml)	C _{NaOH} (M)	m (gm)	AC %	Average AC%
0	2.42	0.1	0.1	38.72	38.93
0	2.45	0.1	0.1	39.2	
0	2.43	0.1	0.1	38.88	

Table 1. Volumetric titration of oxidized dialdehyde-cellulose (DAC) for average aldehyde content percentage AC% estimation.

Physicochemical properties of native cellulose, DAC@CAH, and DAC@CAH@SK₂ composite

Specific surface area is an essential parameter, as it has a great effect on adsorbent capacity toward pollutants. The surface area of DAC, DAC@CAH, and DAC@CAH@SK₂ was measured and is presented in Table 2. The surface area was decreased by modification of cellulose with cyanoacetohydrazide to 8.137 m²/g. This decrease may be due to the reaction of cyanoacetohydrazide with the cellulose. While the surface area increased after the reaction with CS₂ to 268.729 m²/g, which may be returned to the grafting of SH groups into the material.

The solubility of DAC@CAH@SK₂ was studied by utilizing various solvents like sodium hydroxide (0.1–1 M), HCl (0.1–1 M), and ethanol 99.9%. It was noticed that DAC@CAH@SK₂ is not soluble in any of the utilized solvents.

Characterization*Elemental analysis*

Table 3 illustrates the EA results of native cellulose, DAC@CAH, and DAC@CAH@SK₂ composite. The results obtained indicate that the nitrogen content significantly increased to 11.73% after the modification that occurred through the cellulose oxidation followed by condensation with cyanoacetohydrazide. Nitrogen content decreased to 8.43% with increasing sulfur content to 12.86% after the reaction with Carbon disulfide. These results confirm that DAC-CAH and DAC@CAH@SK₂ are successfully formed. The concentration of the inserted cyanoacetohydrazide units was calculated to be approximately 1.557 mmol g⁻¹.

Scanning electron microscope (SEM)

Surface morphologies of DAC, DAC@CAH, DAC@CAH@SK₂, and DAC@CAH@SK₂-Hg²⁺ are shown in Fig. 3a–d, respectively. Figure 3a and b showed that DAC@CAH has more roughness than DAC material which may be attributed to the chemical modification by cyano-aceto hydrazide. DAC@CAH@SK₂ has more roughness and porous surface than DAC@CAH as shown in Fig. 3c, which may be attributed to the modification of DAC@CAH with CS₂ in the presence of KOH. As shown in Fig. 3d, the SEM of DAC@CAH@SK₂-Hg²⁺ shows a brighter surface than the other materials because mercury has better electric conductivity than the modified cellulose materials^{50,51}.

FTIR spectra

FTIR spectra of native cellulose, its derivatives (DAC, DAC@CAH, and DAC@CAH@SK₂ composite), and DAC@CAH@SK₂-Hg²⁺ are represented in Fig. 4. Native cellulose (Fig. 4a) showed a number of distinctive peaks as the C–O stretching vibrations that appeared in the range of 1000–1200 cm⁻¹. While those in the range of 1260–1410 cm⁻¹ and 3200–3600 cm⁻¹ are assigned to OH bending and stretching vibrations, respectively. Moreover, the peaks of C–H stretching vibrations that are present between 2700 and 3000 cm⁻¹. FT-IR spectrum of DAC is present in Fig. 4b and exhibits a new peak at about 1730 cm⁻¹ which may be assigned to the C=O stretching vibrations of the aldehyde group (RCHO)⁴⁰. DAC Modification with Cyanoacetohydrazide results in some shifts in the IR spectrum of the DAC@CAH, an observed peak at about 1680 cm⁻¹, which may be returned to C=N formation between the DAC' aldehyde groups present and amino groups of the added Cyanoacetohydrazide as present in Fig. 4c and²³. Moreover, the peak between 3600 and 3100 cm⁻¹ became broader due to the OH and amino groups' absorption peaks overlapping⁵². The spectrum of the DAC@CAH@SK₂ composite, Fig. 4d, shows the presence of cyano group stretching vibrations at about 2174 cm⁻¹ that may be appeared after the reaction with CS₂ because of the tautomerism phenomenon⁵³. Furthermore, due to the presence of overlapping bands at the range of 500–600 cm⁻¹, the C–S peak was not visible individually⁵⁴. The second derivative FT-IR was obtained in the 1300–500 cm⁻¹ range to confirm the presence of C–S characteristic peak. As presented in Fig. 5 for DAC@CAH@SK₂ through the 2nd derivative, a band at 590 cm⁻¹ attributed to C–S stretching vibrations was detected^{55,56}.

¹H-NMR

Besides the XRD technique, both liquid and solid phases of NMR are used to study the cellulose structure. Also, the solid phase of ¹³C NMR is used to investigate the various cellulose polymorphs but it is less available and

Sample	Surface area, m ² g ⁻¹
Native cellulose	10.4
DAC@CAH	8.137
DAC@CAH@SK ₂	268.729

Table 2. Surface area of the native cellulose and the prepared materials.

Material	C%	H%	N%	S%
Native cellulose	44.5	7.14	0	0
DAC@CAH	46.93	5.63	11.73	0
DAC@CAH@SK ₂	33.72	3.64	8.43	12.86

Table 3. Elemental analysis of native cellulose and the prepared compounds.

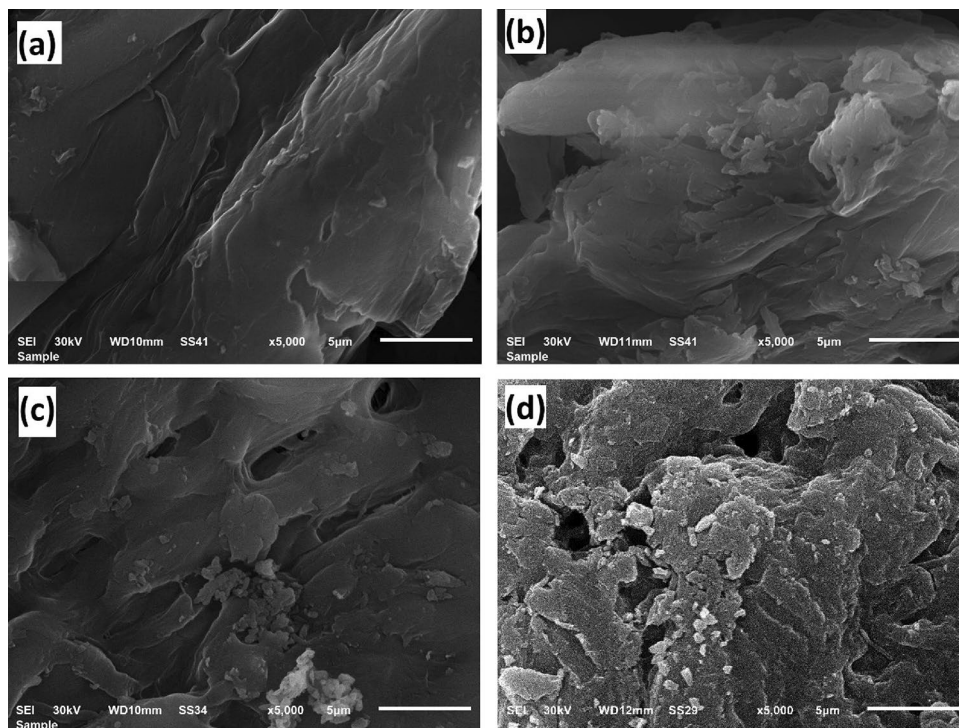


Figure 3. (a) Oxidized cellulose (DAC), (b) DAC@CAH, (c) DAC@CAH@SK₂, and (d) DAC@CAH@SK₂-Hg²⁺.

requires more extensive investigations than liquid phase NMR^{40,57,58}. In all molecular solvents, both DAC and DAC@CAH@SK₂ cellulosic materials are completely insoluble. The ¹H NMR of DAC and DAC@CAH@SK₂ were investigated by utilizing the DMSO/Trifluoroacetic acid mixture⁵⁸. Figure 6 represents the ¹H NMR of DAC and DAC@CAH@SK₂. The ¹H NMR of DAC present in Fig. 6a showed a peak at 2.03 ppm related to the proton that is present on C₂ or C₃ of the DAC. Broad peaks that appeared at 4 ppm and 4.96 ppm are related to C₁ proton and OH, respectively. Figure 6b represents the ¹H NMR of DAC@CAH@SK₂ that showed a new prominent peak, broad signal near 9.28 ppm that could be related to protons of NH of the cyanoacetylhydrazone^{40,59}.

Thermal analysis (TGA)

Thermogravimetric analyses for the DAC@CAH@SK₂ before and after mercury ions adsorption were carried out in the temperature range of 30–900 °C to give information about materials thermal stability, Fig. 7 The thermograms demonstrated that each compound undergoes a series of different degradation steps. The thermal degradation of DAC@CAH@SK₂ and DAC@CAH@SK₂-Hg²⁺ were studied under the same conditions and the total residues were determined as following 27.89% and 21.15%, respectively. The lower value of total residues of DAC@CAH@SK₂-Hg²⁺ compared to the parent one (DAC@CAH@SK₂) suggests that mercury ions show a noncatalytic degradation effect during their complexation with the modified cellulose material⁶⁰.

X-ray diffraction

The diffractograms of the untreated cellulose, DAC, and DAC@CAH@SK₂ are presented in Fig. 8. Key diffraction peaks of the cellulose were shown in the XRD patterns at roughly 15.178°, 16.59°, 20.5°, 22.835°, 28.05°, and 34.475°, with major intensities at peak values of 15.178°, 16.59°, 22.835°, and 34.475°. The primary peaks associated with crystallographic planes were (1 $\bar{1}$ 0), (110), (200), and (004), respectively and these peaks were discovered to be related to cellulose type I^{61–63}. The positions of these investigated peaks stay similar in DAC and DAC@CAH@SK₂ materials with some slight shifting in addition to the samples' crystallinity indices (CrI) were calculated according to the Segal method (Eq. 5) and found to be 73.19, 71.77, and 69.04% for untreated cellulose, DAC, DAC@CAH@SK₂. This may indicate that the crystallinity of the functionalized samples (DAC and DAC@CAH@SK₂) was slightly affected by the adopted chemical modification^{40,64}. The crystallinity decrease is returned to the glucopyranose ring opening and cellulose backbone destruction that result from cellulose oxidation by the KPI and 2,3 dialdehyde cellulose (DAC) formation^{65,66}. The (CrI) value of DAC@CAH@SK₂ is lower than that of DAC which indicates that the DAC@CAH@SK₂ is more amorphous than DAC. This could be illustrated according to their chemical structure as the DAC@CAH@SK₂ has a more compact structure than the DAC^{40,64}.

$$\text{CrI}\% = \frac{I_{200} - I_{am}}{I_{200}} \times 100 \quad (5)$$

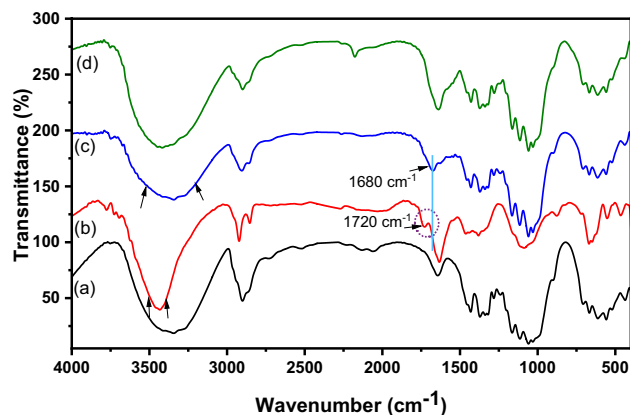


Figure 4. FTIR spectra of (a) native cellulose, (b) DAC, (c) DAC@CAH, and (d) DAC@CAH@SK₂.

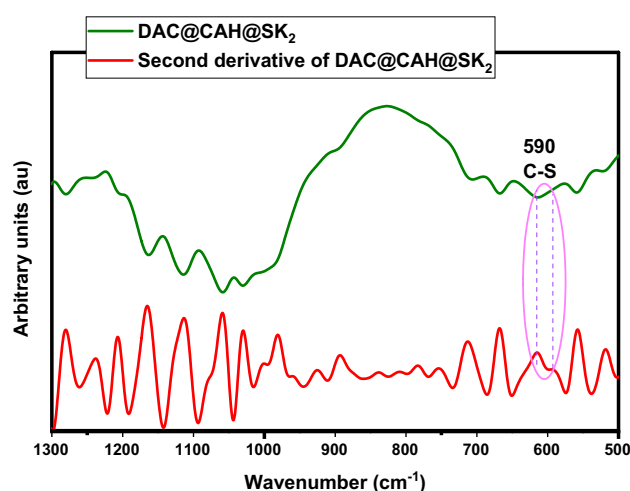


Figure 5. Second derivative spectra of DAC@CAH@SK₂.

As I_{200} and I_{am} are the maximum intensity of 200 diffraction plane at $2\theta = 22.835^\circ$ and the diffraction intensity of the amorphous phase at 2θ of 15.178° , respectively.

Adsorption studies

Point of zero charge (pH_{PZC})

In order to understand the Hg(II) adsorption mechanism by the prepared composite, the point of zero charge of DAC@CAH@SK₂ composite was studied as presented in Fig. 9. This investigation was obtained by measuring the pH at the point of zero charge (pH_{PZC}). Commonly, the chelating agent will show greater affinities for cations at a pH value higher than the value of its pH_{PZC} and vice versa. The pH_{PZC} value obtained for the DAC@CAH@SK₂ composite was approximately 6.85. Hg(II) adsorption by the DAC@CAH@SK₂ was expected to be enhanced at a pH value higher than the pH_{PZC} value.

Effect of pH

The pH is considered an essential parameter as it can influence the solubility and the ionization degree of the studied chelating agent. Also, it can affect metal ion speciation. The adsorption behavior of DAC@CAH@SK₂ chelating agent has been investigated at the pH range of 1–10, which was selected to avoid metal precipitation that occurs in the very alkaline medium. The experiment was studied using 0.01 g of DAC@CAH@SK₂ composite immersed in 10 mL of 150 ppm Hg(II) solution for 180 min. As shown in Fig. 10, the Hg²⁺ adsorption increased with pH increasing from 1 to 5 and became constant at pH range 5–8 then it decreased at pH higher than 8.

The prevailing species for the divalent mercury At pH 2 are HgCl₂, HgCl⁺, Hg²⁺, and HgOHCl by percent % 63.25, 25.20, 3.9, and 2, respectively; in addition to the presence of HgOH⁺ and Hg(OH)₂ in very minor quantities. While the prevailing species at pH 4 are 39.90% Hg(OH)₂, 25.20% HgOHCl, and 10.02% HgCl₂ besides the other species that are present in very small percent such as HgOH⁺, HgCl⁺, and Hg²⁺. The Hg(OH)₂ and HgOHCl species are the prevalent ones at the pH range from 6 to 8 and present by percent 79.62% and 10.02%, respectively^{67–69}. The higher affinity of the DAC@CAH@SK₂ composite to Hg(II) at higher pH is that the prepared composite contains SK groups that consider soft bases while Hg(II) ions are soft acids. In accordance with the

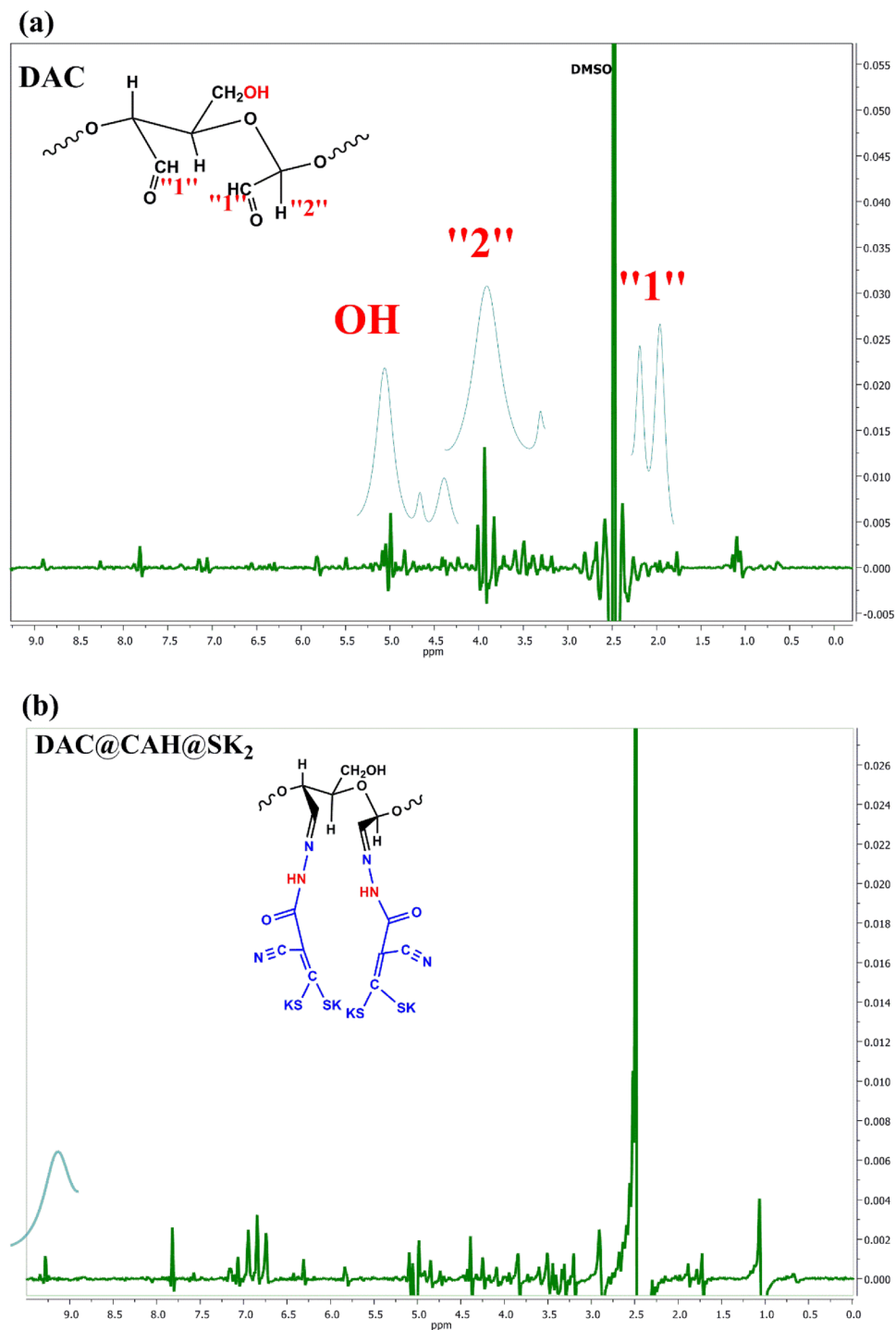


Figure 6. ^1H NMR of (a) DAC and (b) DAC@CAH@SK₂.

theory of Pearson, throughout an acid–base reaction hard acid coordinates with the hard base while soft acid coordinates with the soft base. Neutral molecules consider softer acids.

Our experimental results indicate that the pH is a major parameter in Hg(II) adsorption process by the DAC@CAH@SK₂ composite. The Hg(II) adsorption to cellulose-based adsorbents in response to pH changes has been investigated by several researchers. Bisla et al.⁷⁰ investigated the Hg(II) adsorption by 1-methionine-functionalized cellulose nanofibers adsorbent which has pHPzc equals 7.8 in the pH range (2–10) and declared the very low Hg(II) adsorption capacity at pH value 2, then a constant adsorption capacity increase in the range of pH 4–8, and then followed by a slight decrease at pH value 10. Arias et al.⁷¹ reported that the Hg(II) removal % by lignocellulosic materials was very low at pH 2 and then increased relatively up to pH 9. Anirudhan and Shainy⁶⁷ investigated the divalent Hg ions adsorption into 2-mercapto benzamide-modified nano cellulose composite

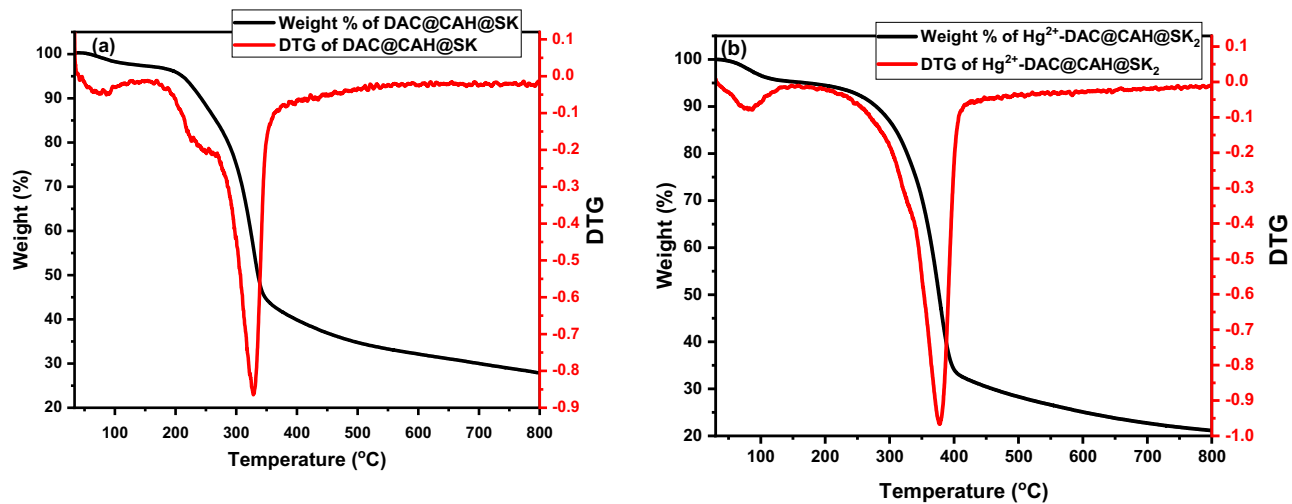


Figure 7. Thermal analysis of (a) DAC@CAH@SK₂ and (b) DAC@CAH@SK₂.Hg²⁺.

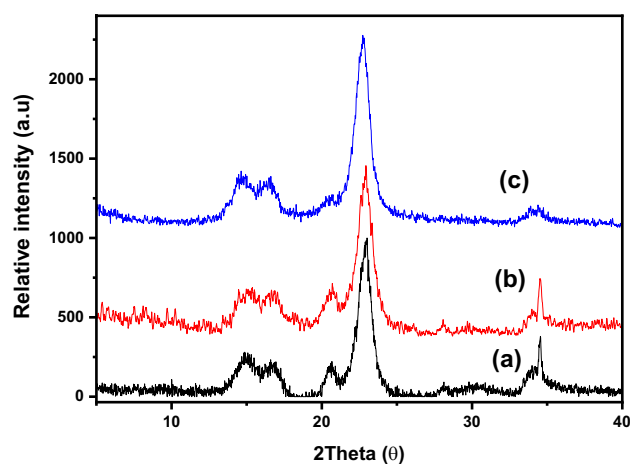


Figure 8. XRD patterns of (a) Cellulose, (b) DAC, and (c) DAC@CAH@SK₂.

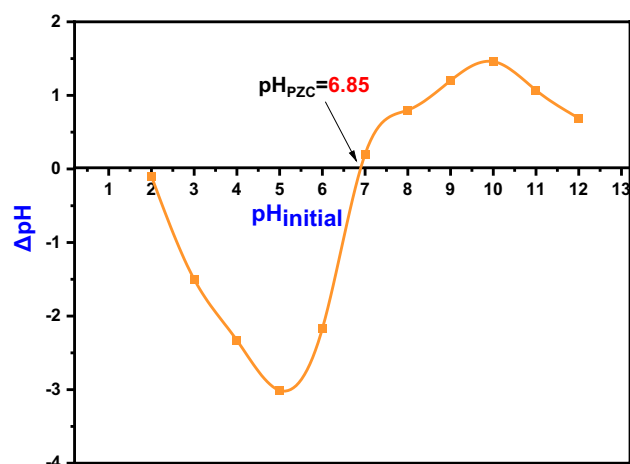


Figure 9. pH_{PZC} of the DAC@CAH@SK₂.

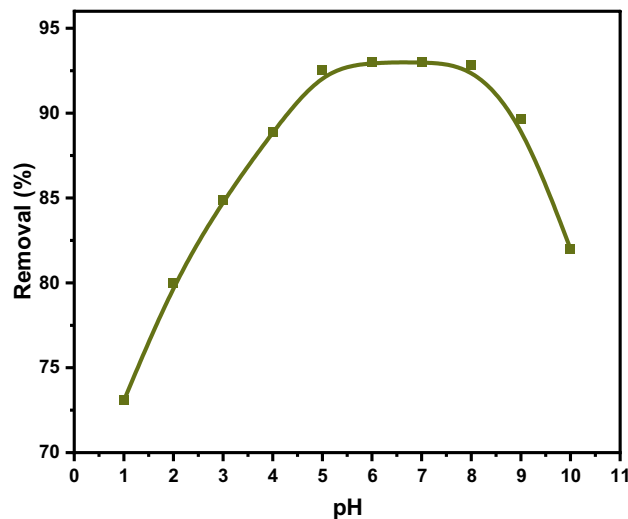


Figure 10. pH effect on Hg^{2+} adsorption onto DAC@CAH@SK₂.

with a pH_{pzc} value equal to 6.5 in the pH range of 3–11. They indicated that the divalent mercury adsorption increased by pH value increasing from 3 to 8 and then decreased sharply as the pH value increased to 11. These investigations recommend that $\text{Hg}(\text{II})$ adsorption to cellulose-based adsorbents relies on the utilized adsorbent/chelating agent properties such as pH_{pzc} , functional groups, etc. in addition to the speciation of the divalent mercury in the studied solution.

Effect of chelating agent dose

The influence of DAC@CAH@SK₂ composite dose on Hg^{2+} adsorption capacity (mg/g) and removal efficiency (%) was obtained by utilizing various doses of it and the results are present in Fig. 11. The Hg^{2+} removal % increased rapidly as the chelating agent dosage increases from 0.001 to 0.01 g, with an increase in the adsorption capacity from 110 to 139.5 mg/g. While the removal % slightly increased from 93 to 97% by increasing the DAC@CAH@SK₂ composite dose from 0.01 to 0.015 g this was accompanied by a decrease in adsorption capacity from 139.5 to 97 mg/g. This may be returned to the increase in DAC@CAH@SK₂ dose results in the specific surface area increase which means more available adsorption sites.

Effect of initial concentration of Hg^{2+}

To investigate the effect of initial concentration on Hg^{2+} adsorption capacity, a 10 ml solution of Hg^{2+} at a fixed-dose of DAC@CAH@SK₂ chelating agent 0.01 g for Hg^{2+} was taken at pH 6 for 3 h in range (25–400 ppm). After that, initial concentrations were varied and the corresponding capacities and removal percentages were obtained as shown in Fig. 12. It was noticed that the DAC@CAH@SK₂ adsorption capacity for Hg^{2+} increased from 24.88

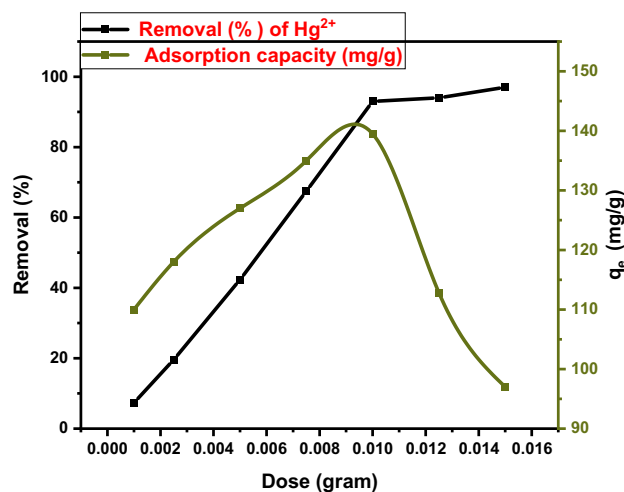


Figure 11. Effect of sorbent dose on adsorption of Hg^{2+} (conditions: 10 ml aqueous solution of 150 mg/L for Hg^{2+} solution for 3 h at pH 6).

to 139.1 mg/g with Hg^{2+} initial concentration increasing from 25 to 150 ppm. Moreover, with the increase of Hg^{2+} initial concentration from 150 to 400 ppm, the DAC@CAH@SK₂ composite tends to stabilize.

Adsorption isotherms

The adsorption isotherm can be defined as follows; the studied adsorbate concentration relation with the adsorbed pollutant amount (q_e) at the adsorbent (chelating agent) surface at a fixed temperature. Dubinin–Radushkevich (D-R), Langmuir, and Freundlich's isothermal models, which can indicate the maximum adsorption capacity (q_e) and binding affinity, were applied in the linear form and the parameters were determined as present in Eqs. (6), (7) and (8), respectively. The dimensionless equilibrium factor (R_L) presented in Eq. (9), is an important parameter that is used in adsorbent-sorbate affinity prediction. Its values are explained as follows: if the R_L value is found to be greater than 1.0 this means that the investigated material is unsuitable and unfavorable, while if it is found to be ($0 < R_L < 1$), ($R_L = 0$), or ($R_L = 1$) this means the reaction is favorable, irreversible, or linear, respectively^{23,35}. The Dubinin–Radushkevich model studies adsorption energetically and creates the assumption that the adsorption process relates to pore volume and surface porosity. Equation (10) represents the E_{DR} which can be defined as following the adsorption mean free energy obtained from the D–R model. It reveals whether the adsorption process is chemical ($8 < E_{DR} < 16 \text{ kJ mol}^{-1}$) or physical (E_{DR} is lower than 8 kJ mol^{-1})⁴⁰.

$$\ln q_e = \ln q_m - k\varepsilon^2 \quad (6)$$

$$\frac{C_e}{q_e} = \frac{1}{K_L q_m} + \frac{C_e}{q_m} \quad (7)$$

$$\ln q_e = \ln K_f + \frac{1}{n} \ln C_e \quad (8)$$

$$R_L = \frac{1}{1 + K_L C_o} \quad (9)$$

$$E_{DR} = \frac{1}{\sqrt{2K}} \quad (10)$$

where C_e (mg/L), $1/n$, K_L (L/mg), K_f (mg/g), and K are the Hg^{2+} concentration at equilibrium, the heterogeneity factor, Langmuir, Freundlich, and the Dubinin–Radushkevich constants, respectively. While, q_e and q_m , which are expressed in mg/g, are the Hg^{2+} capacity at equilibrium and adsorption maximum amount. R which its value equals 8.314 J/mol and T which is expressed in Kelvin are the gas constant and the temperature, respectively. ε is the adsorption potential and is presented in Eq. (11).

$$\varepsilon = RT \ln \left(1 + \frac{1}{C_e} \right) \quad (11)$$

The Langmuir, Freundlich, and D–R isotherms determined for the Hg(II) adsorption utilizing DAC@CAH@SK₂ chelating agent are presented in Fig. 13 and their derived parameters (K_L , K_f , K , n , and q_m) are given in Table 4. The Hg(II) adsorption process using DAC@CAH@SK₂ composite follows the Langmuir isotherm model as the R^2 value for the Langmuir isotherm model is higher than that of Freundlich as presented in Table 4. This explains that the binding of Hg(II) ions to the active sites of the DAC@CAH@SK₂ composite is a chemisorption

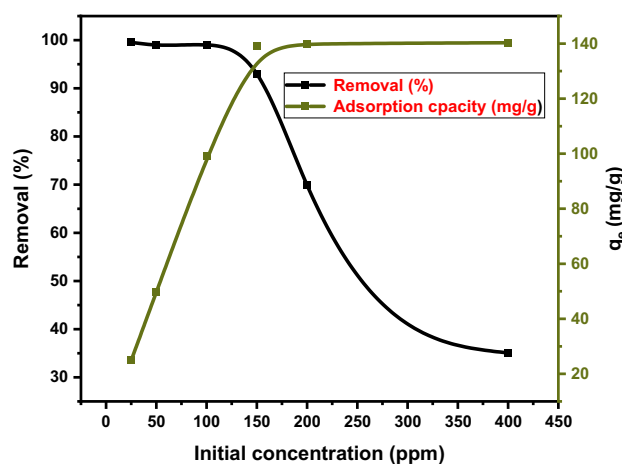


Figure 12. Effect of Hg^{2+} initial concentration (conditions: 0.01g of DAC@CAH@SK₂ was taken at pH 6 for 3 h in range 25 ppm–400 ppm of Hg^{2+}).

Material	Langmuir isotherm constants			
	K_L (L/g)	q_m (mg/g)	R^2	R_L
DAC@CAH@SK ₂ -Hg ²⁺	2.777	140.65	1	0.0024
Material	Freundlich isotherm constants			R^2
	K_F	n		
DAC@CAH@SK ₂ -Hg ²⁺	1.22	0.2416		0.72685
Material	D-R isotherm constants			
	K	E (kJ/mole)	q_m (mg/g)	R^2
DAC@CAH@SK ₂ -Hg ²⁺	5.156×10^{-9}	9.847	108.58	0.72272

Table 4. Adsorption isotherm parameters of Hg(II) by DAC@CAH@SK₂.

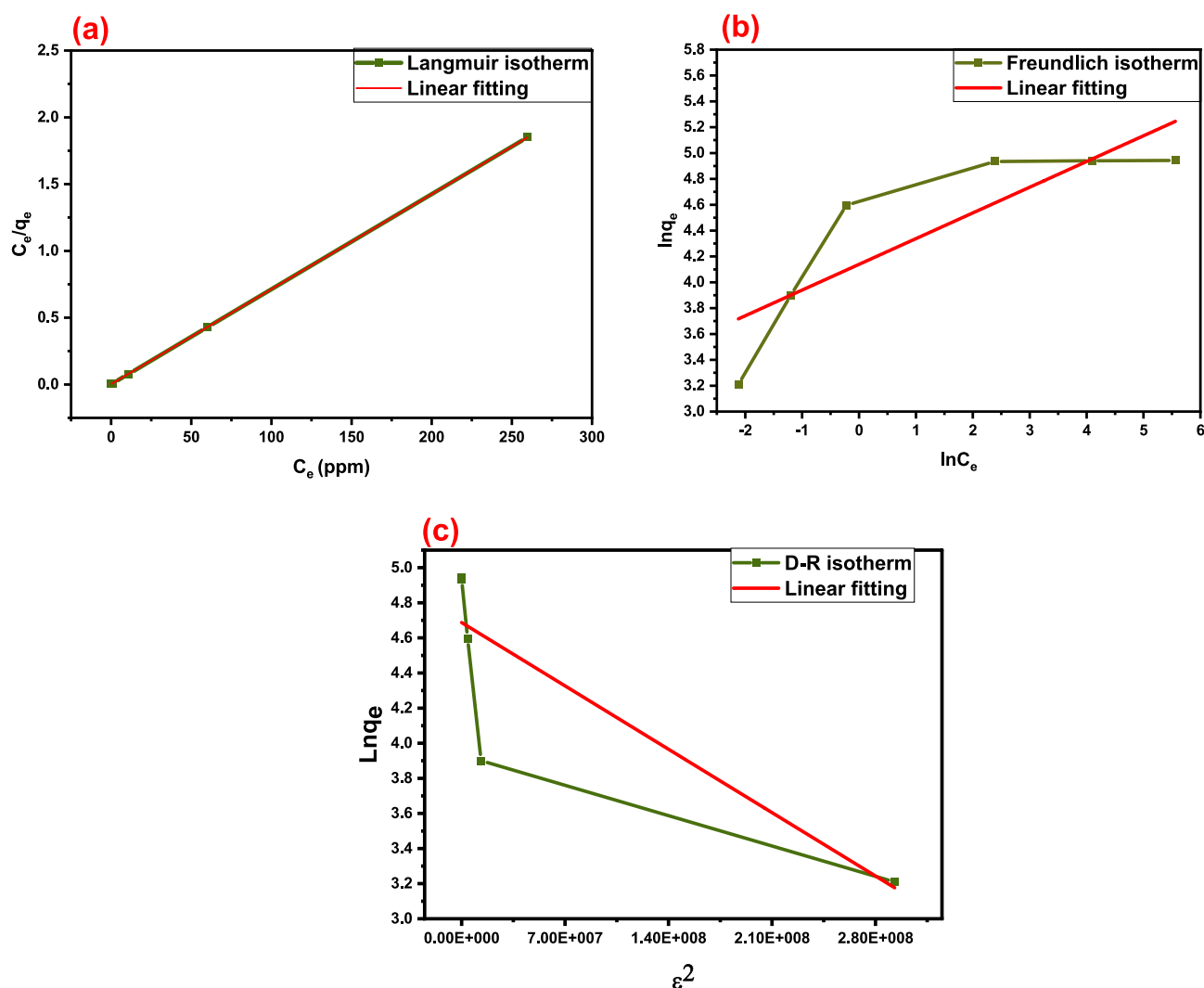


Figure 13. Adsorption isotherms for Hg(II) adsorption by DAC@CAH@SK₂: (a) Langmuir isotherm model, (b) Freundlich isotherm model, and (c) D-R isotherm model.

process (mono-layer). The R_L value was calculated and found to lie between 0 and 1 as shown in Table 4 which implies that the Hg(II) adsorption by DAC@CAH@SK₂ composite is a favorable process that proves the applicability of the prepared composite for Hg(II) remediation from solutions⁴⁰. The current adsorption process' E_{DR} was calculated from the D-R model as presented in Eq. (10) and found to be 9.847 lies in the range of 8–16 kJ mol⁻¹ which reveals that the Hg(II) adsorption process onto the DAC@CAH@SK₂ composite was chemisorption⁴⁰.

Effect of oscillation time and adsorption kinetics

In order to investigate the Hg(II) adsorption mechanism using the DAC@CAH@SK₂ material, the kinetic studies have occurred by examining the influence of oscillating time at various times from 30 to 300 min using 0.01 g of DAC@CAH@SK₂ which was added to a series of glass bottles contain 10 ml of 150 ppm Hg(II). Figure 14a illustrates the adsorption capacity of DAC@CAH@SK₂ at different oscillating times. It is noticed that the adsorption capacity of DAC@CAH@SK₂ increased with the increase of oscillating time from 30 to 180 min to reach q_e value 139.5 mg/g. At an oscillating time of 180 min, the DAC@CAH@SK₂ adsorption capacity became constant and the Hg(II) adsorption attained equilibrium.

In order to determine the Hg²⁺ adsorption rate-limiting step, kinetic investigations were carried out using three typical models; pseudo-1st-order, pseudo-2nd-order and the intraparticle diffusion model (IPD) model which are shown in Eqs. (12), (13) and (14), respectively.

$$\frac{1}{q_{t(\text{ads})}} = \frac{k_1}{q_{e(\text{ads})}} t + \frac{1}{q_{e(\text{ads})}} \quad (12)$$

$$\frac{t}{q_{t(\text{ads})}} = \frac{1}{k_2 q_{e(\text{ads})}^2} t + \frac{1}{q_{e(\text{ads})}} t \quad (13)$$

$$q_t = k_{\text{diff}} * t^{0.5} + C \quad (14)$$

The adsorption efficiency for Hg²⁺ at equilibrium and at a certain time t (min) are expressed as q_e (mg/g) and q_t (mg/g), respectively. As well as K_1 , K_2 , and K_{diff} are pseudo-1st-order, pseudo-2nd-order, and IPD constants, respectively. The C which is defined as the IPD equation intercept, was utilized in order to investigate the impact of the boundary layer. It was discovered that as the intercept value increased, the contribution of the rate-limiting step got higher.

Figure 14b–d presents the experimental data fitting to Pseudo-1st-order (PFO), Pseudo-2nd-order (PSO), and Intraparticle-diffusion (IPD) kinetic models. Moreover, the kinetic parameters (K_1 , K_2 , K_{diff} , q_e , q_e^2 , and R^2) derived from the three models are shown in Table 5. The adsorption of Hg(II) by DAC@CAH@SK₂ achieved equilibrium within 3 h (Fig. 14a). When the correlation coefficients, R^2 , of both PFO and PSO models were compared, it was discovered that the results fit the PSO kinetic model better. It was noticed that two-line components appeared rather than a single one passing through the origin in the IPD model graph (Fig. 14d), which indicates that Hg²⁺ adsorption onto DAC@CAH@SK₂ composite includes different diffusion stages that take place on and inside the DAC@CAH@SK₂ surface. In this case, it was demonstrated that it is not possible to describe the adsorption with one kinetic model. The IPD model for Hg²⁺ adsorption by the DAC@CAH@SK₂ composite indicates that the adsorption provides various diffusion stages that occurred on the DAC@CAH@SK₂ composite surface and inside its surface. In the beginning, numerous active sites were available so the adsorption occurred quickly. Then, with oscillating time passing the DAC@CAH@SK₂ composite active sites decreased and the diffusion of Hg²⁺ into pores becomes more difficult so the adsorption becomes slower^{40,72,73}.

Thermodynamics

To study the nature of the Hg²⁺ adsorption process onto the DAC@CAH@SK₂ surface in terms of spontaneity and feasibility and to estimate the degree of randomness at the solid/liquid interface, adsorption thermodynamic parameters (ΔG_{ads}^0 , ΔH_{ads}^0 , and ΔS_{ads}^0) were determined at a temperature range (of 25–45 °C). Where ΔG_{ads}^0 , ΔH_{ads}^0 , and ΔS_{ads}^0 are Free energy, the heat of enthalpy, and adsorption entropy, respectively. Hg²⁺ adsorption by DAC@CAH@SK₂ material was determined ΔG_{ads}^0 parameter was calculated from the following equations Eqs. (15), (16), and (17). The plotting of $\ln K_C$ vs $(1/T)$ temperature in Kelvin for the Hg²⁺ adsorption onto the DAC@CAH@SK₂ composite is presented in Fig. 15.

$$K_C = \frac{C_{\text{ad}}}{C_e} \quad (15)$$

$$\Delta G_{\text{adsn}}^0 = -RT \ln K_C \quad (16)$$

$$\ln K_C = \frac{\Delta S_{\text{adsn}}^0}{R} - \frac{\Delta H_{\text{adsn}}^0}{RT} \quad (17)$$

As K_c , C_{ad} , and C_e are a thermodynamic equilibrium constant, the Hg²⁺ concentration taken by DAC@CAH@SK₂ material at equilibrium (mg/g), and the Hg²⁺ concentration at equilibrium (mg/L), respectively. While R is the universal gas constant.

As presented in Table 6, the negative values of ΔG_{adsn}^0 and ΔH_{ads}^0 demonstrate that Hg²⁺ adsorption by DAC@CAH@SK₂ is spontaneous and exothermic, respectively. While the arrangement increasing and disorder lowering occurrence was proved from the negative value of ΔS_{ads}^0 .

Effect of interfering ions and adsorption selectivity

The selectivity parameter is very essential to evaluate the DAC@CAH@SK₂ composite's adsorption properties^{74,75}. Hence, The DAC@CAH@SK₂ adsorption selectivity for Hg(II) in the presence of different coexisting metal

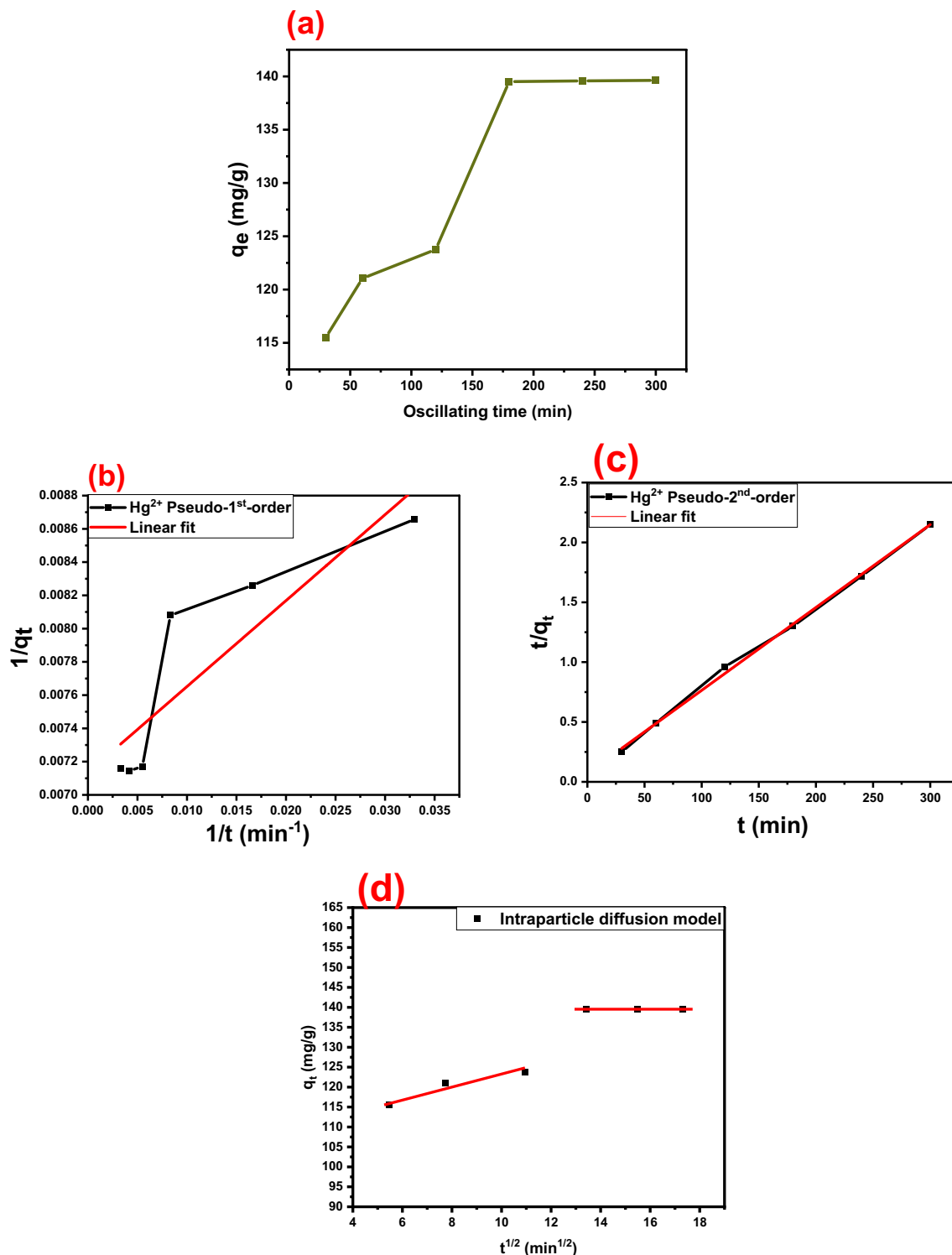


Figure 14. (a) Effect of oscillation time on adsorption of Hg^{2+} (conditions: 0.01 g of DAC@CAH@SK₂, 10 ml of 150 ppm Hg^{2+} , Temp.: 25 °C, time: 30–300 min), (b) Pseudo-1st-order kinetic model for Hg^{2+} adsorption, (c) Pseudo-2nd-order kinetic model for Hg^{2+} adsorption, and (d) IPD kinetic model for Hg^{2+} adsorption.

ions was carried out as shown in Table 7. At the $\text{Hg}(\text{II})$ adsorption optimum conditions, the DAC@CAH@SK₂ composite exhibits excellent selectivity for the $\text{Hg}(\text{II})$ ions with the interfering metal ions (Ni(II), Zn(II), Pb(II), Cu(II), and Cd(II)) either in binary systems or multiple-components synthetic mixtures. DAC@CAH@SK₂ exhibits selective adsorption recovery (Re, %) for $\text{Hg}(\text{II})$ of 100% with the interference of Cu(II), Ni(II), and Zn(II) ions. While DAC@CAH@SK₂ shows recovery higher than 97% in the presence of Cd(II) and Pb(II) ions. This excellent adsorption selectivity of DAC@CAH@SK₂ for $\text{Hg}(\text{II})$ is attributed to the presence of abundant

Material	First-order model		
	K_1 (min^{-1})	$q_{e1\text{ads}}$ (mg/g)	R^2
DAC@CAH@SK ₂ -Hg ²⁺	7.25	141	0.77949
Material	Second-order model		
	k_2 (g/(mg min))	$q_{e2\text{ads}}$ (mg/g)	R^2
DAC@CAH@SK ₂ -Hg ²⁺	5.5677×10^{-4}	146.19	0.9977
Material	Intraparticle diffusion model		R^2
	K_{diff}		
DAC@CAH@SK ₂ -Hg ²⁺	0.388667		0.8961

Table 5. Kinetic parameters for the adsorption of Hg²⁺ by DAC@CAH@SK₂.

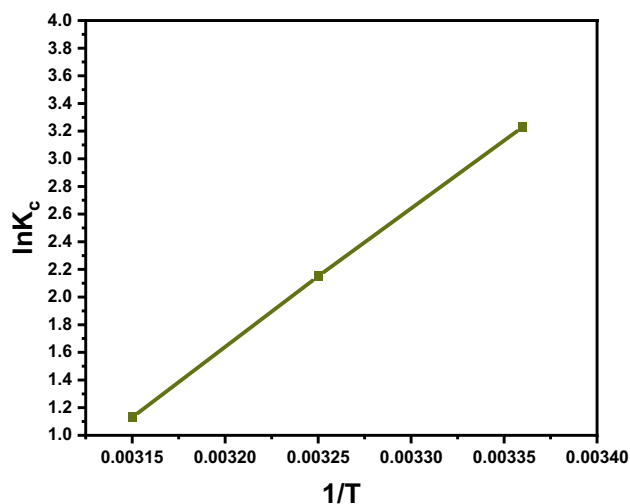


Figure 15. Plot of $\ln K_c$ vs $(1/T)$ absolute temperature for the adsorption of Hg²⁺

System	T (k)	K_c	$\Delta G_{\text{ads}}^{\circ}$ (KJ/mol)	$\Delta H_{\text{ads}}^{\circ}$ (KJ/mol)	$\Delta S_{\text{ads}}^{\circ}$ (J/mol K)
DAC@CAHSK ₂ -Hg ²⁺	298	25.36	-8.00256	-83.115	-252.359
	308	8.584	-5.5055		
	318	3.0956	-2.98755		

Table 6. Thermodynamic parameters for the adsorption of Hg²⁺ onto DAC@CAH@SK₂

nitrogen and sulfur-containing groups such as -NH₂, -NH⁻ and -SK on the surface of DAC@CAH@SK₂, which exhibit strong affinity to Hg(II). When Pb(II) coexists with Hg(II), the selectivity coefficient is quite low, which may be illustrated by the hard-soft acid–base theory (HSAB). Both Hg(II) and Pb(II) are sorted as soft ions which have a strong affinity with thiol and nitrogen active groups that present on the DAC@CAH@SK₂ composite. DAC@CAH@SK₂ demonstrates outstanding recovery (Re, %) for Hg(II) of 102% and 104% in the presence of the following synthetic mixtures (Hg(II), Pb(II), Cd(II), and Zn(II)) and (Hg(II), Pb(II), Cd(II), Zn(II), and Cu(II)), respectively. As a whole, the DAC@CAH@SK₂ composite can potentially adsorb and separate Hg(II) in binary and multiple-metal ions systems. Metal sulfides, dithiocarbamates/thiocarbamates, thiosemicarbazones, thioureas, thiadiazole, and thiazoles are a number of agents that have been well identified for the materials' functionalization for Hg(II) adsorption/uptake. Carbon and sulfur groups are the major components of these agents. Because sulfur is very selective towards mercury, its usage in material modification/functionalization is particularly desirable. Furthermore, Hg(II) forms stable complexes with ligands containing nitrogen and oxygen active groups⁷⁶.

Influence of ionic strength

The parameter of ionic strength was studied by utilizing Cl⁻, I⁻, and NO₃⁻ inorganic electrolytes in the form NaCl, KI, and NaNO₃, respectively. It was investigated by utilizing 0.01 g of DAC@CAH@SK₂ that was added to 10 ml aqueous solution of 100 ppm of Hg(II), at 25 °C for 180 min and investigated electrolytes concentration

System	Metal ions	Added ($\mu\text{g mL}^{-1}$)	Found ($\mu\text{g mL}^{-1}$)	Re (%)	q (mg/g)	Selectivity Coefficient (α)
Hg(II)–Ni(II)	Hg(II)	150	10.5	100	139.50	∞
	Ni(II)	150	150		0.00	
Hg(II)–Cd(II)	Hg(II)	150	20.26	97.1	129.74	∞
	Cd(II)	150	150		0.00	
Hg(II)–Cu(II)	Hg(II)	150	10.51	100	139.49	77.49
	Cu(II)	150	148.2		1.8	
Hg(II)–Zn(II)	Hg(II)	150	10.48	100	139.52	17.66
	Zn(II)	150	142.1		7.9	
Hg(II)–Pb(II)	Hg(II)	150	13.569	97.8	136.43	4.7
	Pb(II)	150	121		29	
Hg(II), Pb(II), Cd(II), Zn(II)	Hg(II)	150	3.871	104.6	146.13	5.7
	Pb(II)	150	135		15	
	Cd(II)	150	150		0.00	
	Zn(II)	150	139.4		10.60	
Hg(II), Pb(II), Cd(II), Zn(II), Cu(II)	Hg(II)	150	7.4	102	142.60	6.956
	Pb(II)	150	136.5		13.50	
	Cd(II)	150	149.8		0.20	
	Zn(II)	150	143.2		6.80	
	Cu(II)	150	150		0.00	

Table 7. Effect of interfering ions on the recovery of Hg(II) by DAC@CAH@SK₂ sorbent.

range between 0 mol/L and 1 mol/L. As shown in Fig. 16, The DAC@CAH@SK₂ adsorption efficiency for Hg(II) declined with the investigated electrolytes (Cl⁻, I⁻, and NO₃⁻) concentration increasing.

Desorption and reusability studies

Different eluents were tried for desorption of Hg²⁺ from the DAC@CAH@SK₂ as ethanol, HCl (0.1 M and 0.2 M), NaOH (0.05 M), NaHCO₃ (0.1 M), K₂CO₃ (0.1 M), thiourea (0.1 M), HNO₃ (0.1 M), 0.1 M thiourea/0.1 M HNO₃ mixture (1:1). It was found that thiourea/HNO₃ mixture (1:1) was the most effective eluent among them and was successfully used for the desorption of the Hg²⁺ from DAC@CAH@SK₂.

The DAC@CAH@SK₂ re-using was studied for five sorption–desorption cycles at the optimum conditions with sorption efficiency higher than 89% as shown in Table 8. It was predicted that DAC@CAH@SK₂ material could be a good sorbent for Hg²⁺ removal from aqueous solutions.

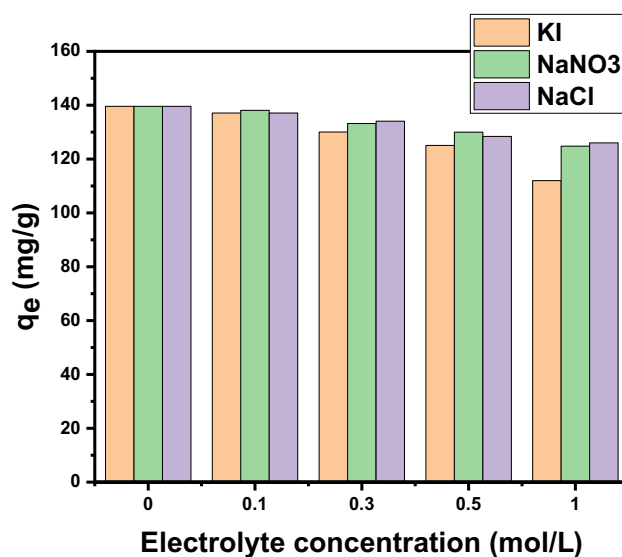


Figure 16. Effect of ionic strength on the Hg(II) adsorption (conditions: 0.01g of DAC@CAH@SK₂ was taken at 10 ml 150 ppm of Hg²⁺ at pH 6 for 3 h).

Applications

The application experiments of the DAC@CAH@SK₂ were obtained by adsorption of Hg²⁺ (100 mg/L and 150 mg/L) from tap water, seawater, and wastewater samples to evaluate prepared chelating agent applicability in real samples. As displayed in Table 9, the Hg²⁺ recoveries (%) from the tested real wastewater samples exceeded 95%. It was demonstrated that DAC@CAH@SK₂ has remarkable recoveries for the Hg²⁺ that was spiked in the tested water samples proving that the DAC@CAH@SK₂ can be used for mercury removal from the aqueous environment in actual practice.

Plausible adsorption mechanism

To investigate the possible mechanism of Hg²⁺ adsorption on DAC@CAH@SK₂, SEM, digital images, and FTIR of the DAC@CAH@SK₂ and Hg²⁺-DAC@CAH@SK₂ were evaluated.

Digital photographs. The digital photographs of native cellulose, DAC, DAC@CAH, DAC@CAH@SK₂, and Hg²⁺-DAC@CAH@SK₂ were shown in Fig. 17a–e, respectively. An obvious color changes after each step, it converted from the white color of the DAC to the pale sandy fawn color after modification with cyano-aceto hydrazide (Fig. 17b and c) and to dark yellow after modification with Carbon disulfide and potassium hydroxide as in Fig. 17d. The color of the modified cellulose changed into greenish yellow after the adsorption of Hg²⁺ as in Fig. 17e. These changes indicated that the tendency of the modified cellulose towards the adsorption of Hg²⁺.

FTIR spectra. In Fig. 18, the DAC@CAH@SK₂ composite spectrum before and after Hg²⁺ adsorption is shown⁵⁴. This showed that after Hg²⁺ adsorption the cyano group peak disappeared and C–S between 500 and 600 cm⁻¹ became broader than those of DAC@CAH@SK₂⁵⁴. The azomethane characteristic peak which appears at 1650 cm⁻¹ as presented in Fig. 18a showed an obvious shift after the complexation with the Hg²⁺ ions to a lower value of 1632 cm⁻¹ as shown in Fig. 18b. Additionally, the bands corresponding to -NH in the DAC@CAH@SK₂ chelating agent were shifted in the spectrum of Hg²⁺-DAC@CAH@SK₂. All previous indications led us to estimate that the complexation may be performed by forming a six-ring complex either by the lone pair of the cyano group's nitrogen atom and lone pair of the carbonyl group or through the -NH and a sulfur group of the C–S. The Hg²⁺ complexation with the DAC@CAH@SK₂ may also carried out through the carbonyl lone pair and the -NH group results in five ring complex formation.

Cycle number	Desorption (%)	Recovery (%)
1	99.12	98.15
2	98.55	97.07
3	94.58	94
4	92.3	91.1
5	90.23	89.18

Table 8. Repeated adsorption–desorption cycles for DAC@CAH@SK₂ regeneration by using 0.1 M thiourea/0.1 M HNO₃ mixture (1:1).

Wastewater samples type & location	Added (µg mL ⁻¹)	Found (µg mL ⁻¹)	qe (mg/g)	Recovery (%)	RSD (%)
Sea water (Marsa Matrouh, Egypt)	0.00	0.00	0.00	0.00	0.00
	50.00	0.45	49.55	99.7	1.17
	100.00	1.02	98.98	99.78	1.21
	150.00	10.3	139.7	100.05	1.25
Tap water (Mansoura university, Mansoura, Egypt)	0.00	0.00	0.00	0.00	0.00
	50.00	0.72	49.28	99.15	1.27
	100.00	1.32	98.68	99.47	1.22
	150.00	10.42	139.58	99.97	1.25
Waste water (Sinbellawin sewage station, Dakahlia,	0.00	0.00	0.00	0.00	0.00
	50.00	0.65	49.35	99.29	1.19
	100.00	1.95	98.05	98.84	1.2
	150.00	17.2	132.8	95.11	1.18

Table 9. Analysis of spiked Hg²⁺ in real wastewater samples by DAC@CAH@SK₂ (n = 3).

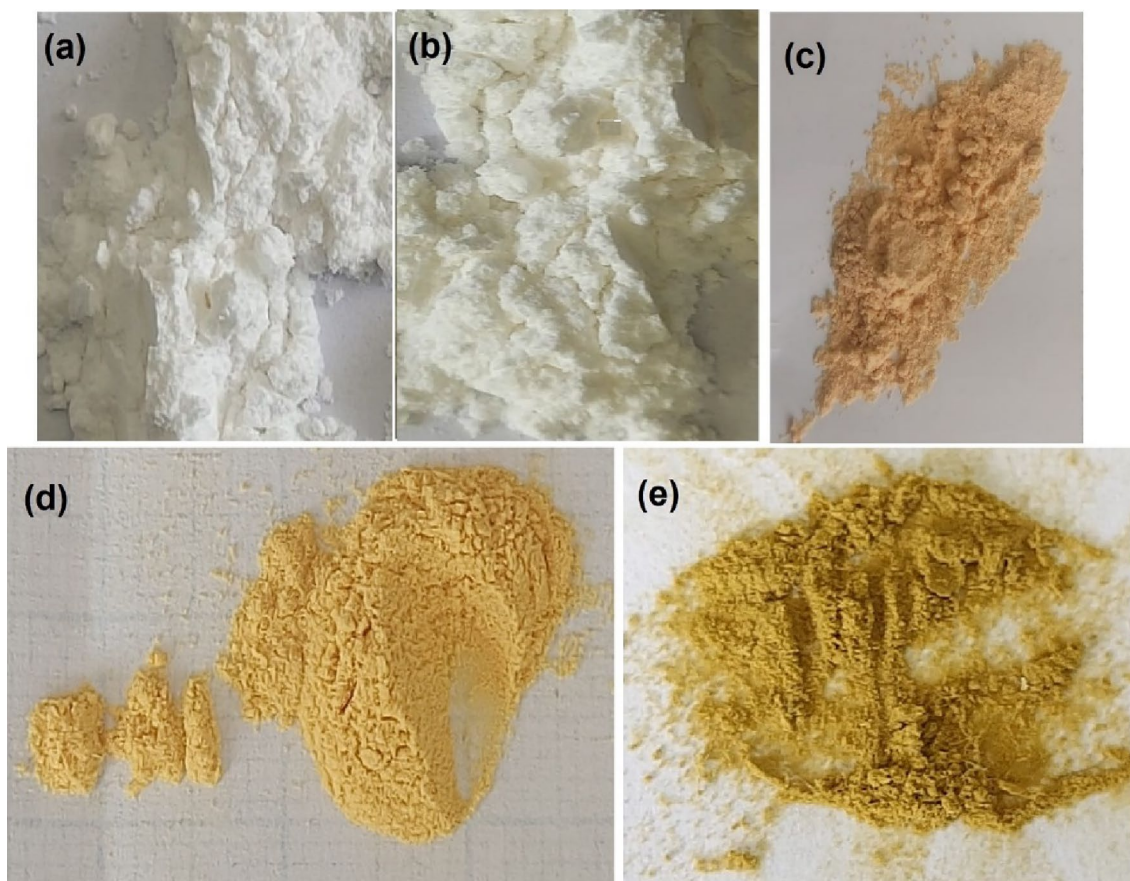


Figure 17. (a) native cellulose, (b) DAC, (c) DAC@CAH, (d) DAC@CAH@SK₂, and (e) Hg²⁺-DAC@CAH@SK₂.

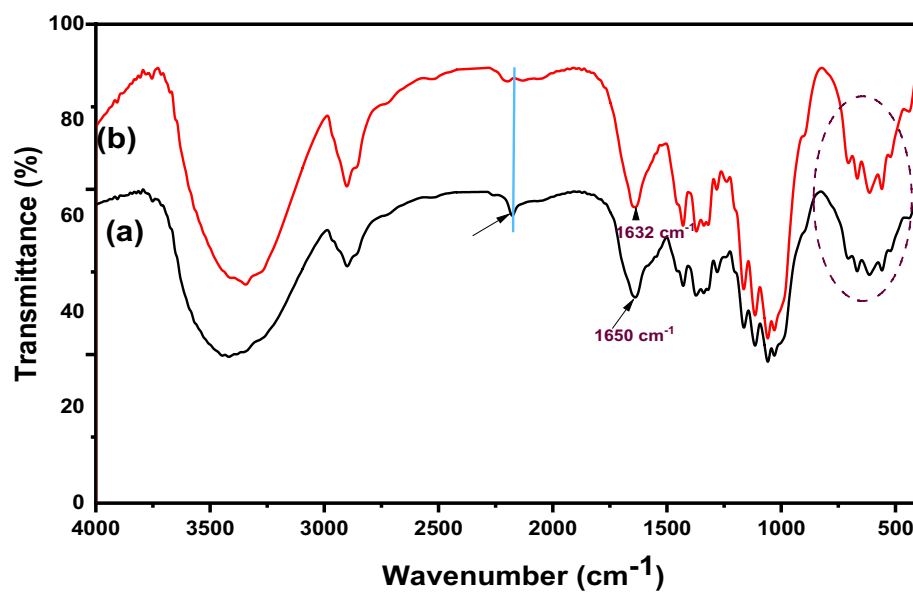


Figure 18. FTIR spectra of (a) DAC@CAH@SK₂ and (b) Hg²⁺-DAC@CAH@SK₂.

Energy-dispersive X-ray spectroscopy (EDS) analysis. The Hg(II) adsorption on the prepared chelating agent surface was confirmed and proved through the energy dispersive X-ray (EDS) analysis investigation as presented in (Fig. 19). The appearance of the Hg(II) characteristic peak in the range 1–3 keV demonstrates the Hg(II) adsorption on the DAC@CAH@SK₂ surface⁷⁷.

Besides the previous evidences, SEM analysis indicates the Hg²⁺ adsorption by the DAC@CAH@SK₂ composite as the surface of the DAC@CAH@SK₂-Hg²⁺ is brighter than that of DAC@CAH@SK₂ as shown in Fig. 3c and d which returns to the mercury electric conductivity properties which result in DAC@SAH@SK₂-Hg²⁺ has better electrical conductivity than the DAC@SAH@SK₂ composite.

The mechanism of any metal ion adsorption onto a material usually is either a chemical reaction or an ion exchange reaction between the chelating agent active groups and the metal ions. Mechanisms applied in Hg(II) adsorption are ion exchange, precipitation, surface-complexation, and complexation/chelation. For thiol (-SH) functionalized adsorbents, the empty orbital of the Hg(II) can bond with free SH lone pair of electrons. Considering the analysis mentioned above, the possible mechanism of Hg(II) ions adsorption onto DAC@CAH@SK₂ composite could be as shown in Fig. 20. The Hg(II) ions complexes were formed via the coordination bonds with -Sk, C=O, C=N, and lone pair of N-H as presented in Fig. 20 forming five-membered ring and six-membered ring stable complexes^{76,78}.

Performance of the prepared DAC@CAH@SK₂

A comparison between DAC@CAH@SK₂ chelating agent' q_{max} (maximum adsorption capacity) for Hg²⁺ with other adsorbents that were previously used for Hg²⁺ pollutant removal was obtained to improve DAC@CAH@SK₂ value as shown in Table 10. We can observe that the Hg²⁺ adsorption by the DAC@CAH@SK₂ is respectably positioned to other researches with a q_{max} of 139.6 at 25 °C since presents a q_{max} value higher than the other reported adsorbents' q_{max}. Because of environmental concerns and development requirements, the desorption process and adsorbent regeneration is an essential matter for any adsorbent to evaluate the adsorbent reusing for industrial applications.

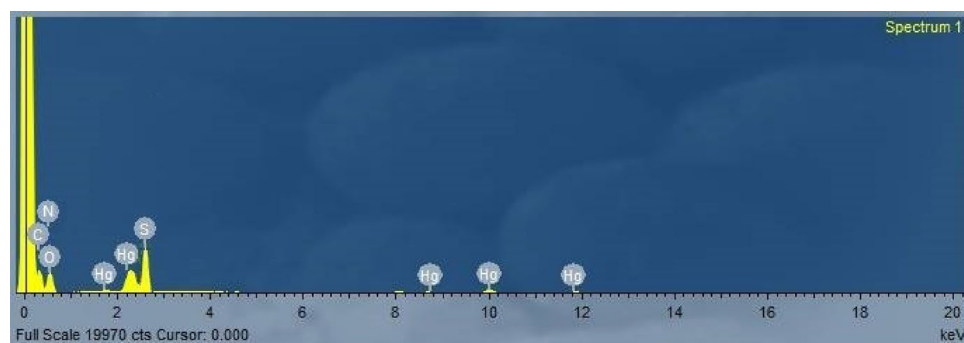


Figure 19. The EDS spectral analysis of DAC@CAH@SK₂-Hg²⁺.

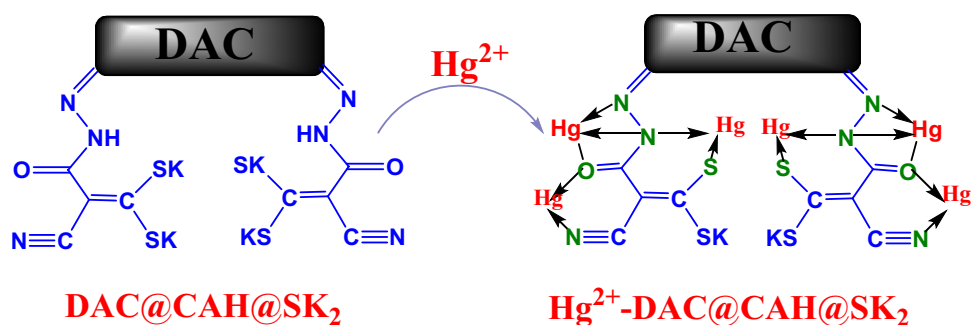


Figure 20. Plausible mechanism of sorption of Hg²⁺ onto DAC@CAH@SK₂.

Adsorbent	Adsorption capacity (mg g ⁻¹)	Equilibrium time (min)	Optimal pH	References
MIL-101-Thymine	52	200	6	79
AMOF-1'	78	1440	–	80
{[Ni1.5(L)(NH ₂ -bpy)-(H ₂ O)]·7.5H ₂ O} _n	93.69	300	3	81
Chitosan derivatives	122.47	–	2	82
Chitosan derivatives	106.4	–	4–6	83
Chitosan fluorescent material	108	30	–	84
Chitosan fluorescent hydrogel	120.79	40	< 3	85
S-SMs	62.3	1500	5.8–8.2	86
Zeolites	22.3	–	2	87
2CFA-derived zeolite	0.3	1 day	2.5	88
Fe ₂ O ₃ @SiO ₂ thin films	126	45	7	89
Bacillus thuringiensis MC28	74	6 days	2–8	90
Sulfurized wood biochar	108	30	6	91
Polyaniline nanoparticles on the polyurethane foam	15	60	7	92
Exhausted coffee waste	32	204	7	93
Mercapto-modified bentonite	16	–	6.17	94
DAC@CAH@SK ₂	139.6	180	5–8	This work

Table 10. Comparison of adsorption capacity and equilibrium time of various adsorbents for Hg²⁺

Conclusion

We demonstrated the fabrication of the DAC@CAH@SK₂ composite and its capability to adsorb Hg(II) metal ions from aqueous solutions. The prepared material was fabricated by oxidation cellulose and subsequent chemical modification processes. The prepared materials (DAC, DAC@CAH, DAC@CAH@SK₂, and DAC@CAH@SK₂-Hg²⁺) were characterized by different techniques such as SEM, TGA, XRD, FT-IR, CHNS, and BET. The DAC@CAH@SK₂ exhibited effective and rapid adsorption behavior toward Hg(II) in aqueous solutions, where the optimal initial pH was 7. The adsorption mechanism was revealed by observing the adsorption isotherm and adsorption kinetics. The equilibrated adsorption capacity as a function of the Hg(II) concentration was described precisely using the Langmuir isotherm model, strongly suggesting that the adsorbates form a monolayer with a homogeneously distributed surface adsorption energy on the DAC@CAH@SK₂ surface. The maximal adsorption capacity obtained from the model was 139.6 mg·g⁻¹ for Hg(II) ions. Kinetic studies with a pseudo-2nd-order kinetic model clearly showed the chemisorption of a single doubly charged mercury ion onto the DAC@CAH@SK₂ composite. In addition to the negative free enthalpy (ΔG°) and enthalpy (ΔH°) values indicated that the adsorption of Hg(II) onto DAC@CAH@SK₂ is spontaneous and exothermic over the investigated temperatures range. The prepared DAC@CAH@SK₂ composite can be utilized effectively for the selective adsorption and

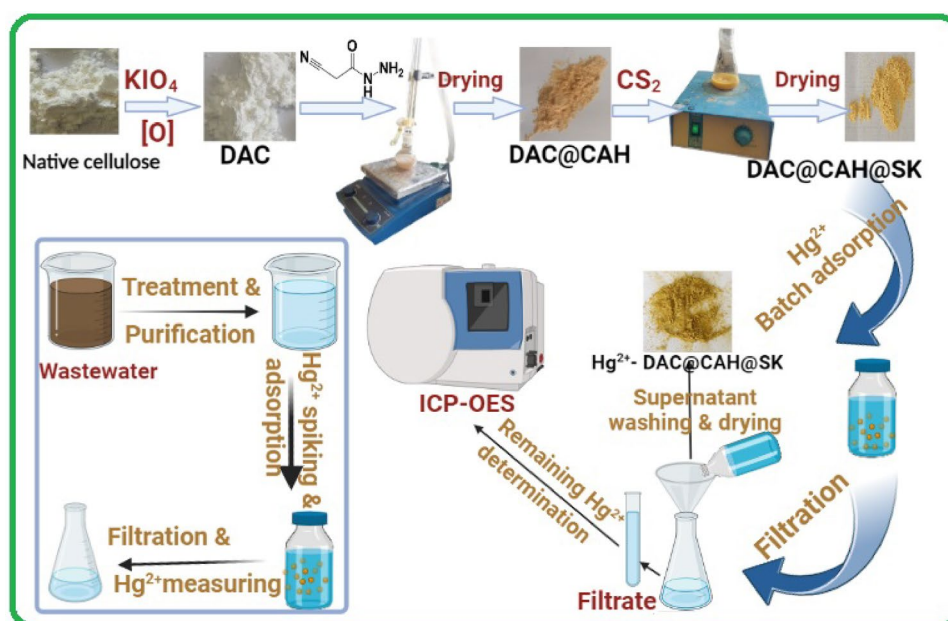


Figure 21. Synthesis of DAC@CAH@SK₂ and its use for Hg²⁺ adsorption.

recovery of Hg(II) ions from aqueous solutions. The comparison of q_e of DAC@CAH@SK₂ composite with other sorbents used in Hg(II) removal was reported in the literature. The DAC@CAH@SK₂ material was applied for the removal of Hg(II) from real waste samples. These results highlight the impact of the chemical surface functionalization of cellulose via oxidation followed by chemical modification toward water remediation. The DAC@CAH@SK₂ Synthesis and its use for Hg²⁺ adsorption is shown in Fig. 21.

Data availability

All data generated or analyzed during this study are included in this published article.

Received: 16 September 2023; Accepted: 27 October 2023

Published online: 09 November 2023

References

- Brohi, R. O. Z., Khuhawar, M. Y., Mahar, R. B. & Ibrahim, M. A. Novel bimetallic nano particles for sorption of mercury(II) from drinking water: adsorption experiment and computational studies. *J. Water Process Eng.* **39**, 101727. <https://doi.org/10.1016/j.jwpe.2020.101727> (2021).
- Zhang, L. *et al.* Adsorption behavior and mechanism of Hg(II) on a porous core-shell copper hydroxy sulfate@ MOF composite. *Appl. Surface Sci.* **538**, 148054. <https://doi.org/10.1016/j.apsusc.2020.148054> (2021).
- Peng, R., Chen, G., Zhou, F., Man, R. & Huang, J. Catalyst-free synthesis of triazine-based porous organic polymers for Hg²⁺ adsorptive removal from aqueous solution. *Chem. Eng. J.* **371**, 260–266. <https://doi.org/10.1016/j.cej.2019.04.063> (2019).
- Xia, J., Wang, Q., Yang, M. & Wu, H. Reliable electroanalysis of Hg(II) in water via flower-like porous MnCo₂O₄: Excellent multi-layer adsorption and (Mn, Co)(II)/(Mn, Co)(III) cycles. *Sens. Actuators B Chem.* **326**, 129008. <https://doi.org/10.1016/j.snb.2020.129008> (2021).
- Zeng, B. *et al.* Facile synthesis of zinc-based organic framework for aqueous Hg(II) removal: Adsorption performance and mechanism. *Nano Mater. Sci.* **3**(4), 429–439. <https://doi.org/10.1016/j.nanoms.2021.06.005> (2021).
- Hu, X., Chen, C., Zhang, D. & Xue, Y. Kinetics, isotherm and chemical speciation analysis of Hg(II) adsorption over oxygen-containing MXene adsorbent. *Chemosphere* **278**, 130206. <https://doi.org/10.1016/j.chemosphere.2021.130206> (2021).
- Shi, M. T., Yang, X. A. & Zhang, W. B. Magnetic graphitic carbon nitride nano-composite for ultrasound-assisted dispersive micro-solid-phase extraction of Hg(II) prior to quantitation by atomic fluorescence spectroscopy. *Anal. Chim. Acta* **1074**, 33–42. <https://doi.org/10.1016/j.aca.2019.04.062> (2019).
- Li, G. P. *et al.* Thiol-functionalized pores via post-synthesis modification in a metal-organic framework with selective removal of Hg(II) in water. *Inorg. Chem.* **58**(5), 3409–3415. <https://doi.org/10.1021/acs.inorgchem.8b03505> (2019).
- Windmüller, C. C. *et al.* The redox processes in Hg-contaminated soils from Descoberto (Minas Gerais, Brazil): Implications for the mercury cycle. *Ecotoxicol. Environ. Saf.* **112**, 201–211. <https://doi.org/10.1016/j.ecoenv.2014.11.009> (2015).
- Tejeda-Benitez, L., Flegal, R., Odigie, K. & Olivero-Verbel, J. Pollution by metals and toxicity assessment using *Caenorhabditis elegans* in sediments from the Magdalena River, Colombia. *Environ. Pollut.* **212**, 238–250. <https://doi.org/10.1016/j.envpol.2016.01.057> (2016).
- Fu, Y. *et al.* New network polymer functionalized magnetic-mesoporous nanoparticle for rapid adsorption of Hg(II) and sequential efficient reutilization as a catalyst. *Sep. Purif. Technol.* **259**, 118112. <https://doi.org/10.1016/j.seppur.2020.118112> (2021).
- Wagner-Döbler, I., Von Canstein, H., Li, Y., Timmis, K. N. & Deckwer, W. D. Removal of mercury from chemical wastewater by microorganisms in technical scale. *Environ. Sci. Technol.* **34**(21), 4628–4634. <https://doi.org/10.1021/es0000652> (2000).
- Alshahrani, A. *et al.* Enhanced heavy metals removal by a novel carbon nanotubes buckypaper membrane containing a mixture of two biopolymers: Chitosan and i-carrageenan. *Sep. Purif. Technol.* **276**, 119300. <https://doi.org/10.1016/j.seppur.2021.119300> (2021).
- Shoneye, A., Sen Chang, J., Chong, M. N. & Tang, J. Recent progress in photocatalytic degradation of chlorinated phenols and reduction of heavy metal ions in water by TiO₂-based catalysts. *Int. Mater. Rev.* **67**(1), 47–64. <https://doi.org/10.1080/09506608.2021.1891368> (2022).
- Tran, T. K., Leu, H. J., Chiu, K. F. & Lin, C. Y. Electrochemical treatment of heavy metal-containing wastewater with the removal of COD and heavy metal ions. *J. Chin. Chem. Soc.* **64**(5), 493–502. <https://doi.org/10.1002/jccs.201600266> (2017).
- Hussain, S. T. & Ali, S. A. K. Removal of heavy metal by ion exchange using bentonite clay. *J. Ecol. Eng.* <https://doi.org/10.12911/22998993/128865> (2021).
- Xue, S. *et al.* Adsorption of heavy metals in water by modifying Fe₃O₄ nanoparticles with oxidized humic acid. *Colloids Surf. A Physicochem. Eng. Asp.* **616**, 126333. <https://doi.org/10.1016/j.colsurfa.2021.126333> (2021).
- Rathi, B. S. & Kumar, P. S. Application of adsorption process for effective removal of emerging contaminants from water and wastewater. *Environ. Pollut.* **280**, 116995. <https://doi.org/10.1016/j.envpol.2021.116995> (2021).
- Chen, H. *et al.* Trash to treasure: From construction waste to tellurium adsorbent materials. *J. Clean. Prod.* **312**, 127752. <https://doi.org/10.1016/j.jclepro.2021.127752> (2021).
- Karimi, F. *et al.* Removal of metal ions using a new magnetic chitosan nano-bio-adsorbent; A powerful approach in water treatment. *Environ. Res.* **203**, 111753. <https://doi.org/10.1016/j.envres.2021.111753> (2022).
- Zhang, G., Lei, B., Chen, S., Xie, H. & Zhou, G. Activated carbon adsorbents with micro-mesoporous structure derived from waste biomass by stepwise activation for toluene removal from air. *J. Environ. Chem. Eng.* **9**(4), 105387. <https://doi.org/10.1016/j.jece.2021.105387> (2021).
- Obijole, O. *et al.* Hydrothermally treated aluminosilicate clay (HTAC) for remediation of fluoride and pathogens from water: Adsorbent characterization and adsorption modelling. *Water Resour. Ind.* **25**, 100144. <https://doi.org/10.1016/j.wri.2021.100144> (2021).
- Akl, M., Ismail, M. A., Hashem, M. A., & Ali, D. A. Novel NS modified cellulose: Synthesis, spectroscopic characterization and adsorption studies of Cu²⁺, Hg²⁺ and Pb²⁺ from environmental water samples (2021).
- Gupta, K., Joshi, P., Gusain, R. & Khatri, O. P. Recent advances in adsorptive removal of heavy metal and metalloid ions by metal oxide-based nanomaterials. *Coord. Chem. Rev.* **445**, 214100. <https://doi.org/10.1016/j.ccr.2021.214100> (2021).
- Gumus, Z. P. & Soyak, M. Metal organic frameworks as nanomaterials for analysis of toxic metals in food and environmental applications. *TrAC Trends Anal. Chem.* **143**, 116417. <https://doi.org/10.1016/j.trac.2021.116417> (2021).
- Zhao, L., Liang, C., Li, S. & Du, K. Study of tentacle-like cationic macroporous cellulose spherical adsorbent for heavy metals. *J. Clean. Prod.* **303**, 127114. <https://doi.org/10.1016/j.jclepro.2021.127114> (2021).
- Xue, F. *et al.* Structural design of a cellulose-based hyperbranched adsorbent for the rapid and complete removal of Cr (VI) from water. *Chem. Eng. J.* **417**, 128037. <https://doi.org/10.1016/j.cej.2020.128037> (2021).
- Ma, J. *et al.* Fast adsorption of heavy metal ions by waste cotton fabrics based double network hydrogel and influencing factors insight. *J. Hazard. Mater.* **344**, 1034–1042. <https://doi.org/10.1016/j.jhazmat.2017.11.041> (2018).

29. Rol, F., Belgacem, M. N., Gandini, A. & Bras, J. Recent advances in surface-modified cellulose nanofibrils. *Prog. Polym. Sci.* **88**, 241–264. <https://doi.org/10.1016/j.progpolymsci.2018.09.002> (2019).
30. Li, Y., Zhu, H., Zhang, C., Cheng, M. & He, H. PEI-grafted magnetic cellulose for Cr(VI) removal from aqueous solution. *Cellulose* **25**(8), 4757–4769. <https://doi.org/10.1007/s10570-018-1868-2> (2018).
31. Rahaman, M. H., Islam, M. A., Islam, M. M., Rahman, M. A. & Alam, S. N. Biodegradable composite adsorbent of modified cellulose and chitosan to remove heavy metal ions from aqueous solution. *Curr. Res. Green Sustain. Chem.* **4**, 100119. <https://doi.org/10.1016/j.crgsc.2021.100119> (2021).
32. Gao, L., Liu, G., Zamyadi, A., Wang, Q. & Li, M. Life-cycle cost analysis of a hybrid algae-based biological desalination–low pressure reverse osmosis system. *Water Res.* **195**, 116957. <https://doi.org/10.1016/j.watres.2021.116957> (2021).
33. Sinha, S. *et al.* Prospects on arsenic remediation using organic cellulose-based adsorbents. *Ind. Crops Prod.* **201**, 116928 (2023).
34. Zhu, G. *et al.* Synthesis of cellulose II-based spherical nanoparticle microcluster adsorbent for removal of toxic hexavalent chromium. *Int. J. Biol. Macromol.* **221**, 224–237 (2022).
35. Akl, M. A., Hashem, M. A., Ismail, M. A. & Abdelgalil, D. A. Novel diaminoguanidine functionalized cellulose: Synthesis, characterization, adsorption characteristics and application for ICP-AES determination of copper(II), mercury(II), lead(II) and cadmium(II) from aqueous solutions. *BMC Chem.* **16**(1), 65 (2022).
36. Tewatia, P., Kaur, M., Singhal, S. & Kaushik, A. Wheat straw cellulose based fluorescent probe cum bioadsorbents for selective and sensitive alleviation of uranium (VI) in waste water. *J. Environ. Chem. Eng.* **9**(5), 106106 (2021).
37. Lei, Z., Gao, W., Zeng, J., Wang, B. & Xu, J. The mechanism of Cu(II) adsorption onto 2,3-dialdehyde nano-fibrillated celluloses. *Carbohydr. Polym.* **230**, 115631 (2020).
38. Gomes, A. S. *et al.* Cationic dialdehyde cellulose microfibers for efficient removal of eriochrome black T from aqueous solution. *Bioresour. Technol.* **380**, 129096 (2023).
39. Akl, M. A. *et al.* Smart guanyl thiosemicarbazide functionalized dialdehyde cellulose for removal of heavy metal ions from aquatic solutions: adsorption characteristics and mechanism study. *Appl. Water Sci.* **13**, 144. <https://doi.org/10.1007/s13201-023-01948-9> (2023).
40. Akl, M. A., El-Zeny, A. S., Hashem, M. A., El-Gharkawy, E. S. R. & Mostafa, A. G. Flax fiber based semicarbazide biosorbent for removal of Cr(VI) and Alizarin Red S dye from wastewater. *Sci. Rep.* **13**(1), 8267 (2023).
41. Antochshuk, V., Olkhoviyk, O., Jaroniec, M., Park, I. S. & Ryoo, R. Benzoylthiourea-modified mesoporous silica for mercury(II) removal. *Langmuir* **19**(7), 3031–3034 (2003).
42. Zhang, L. *et al.* A new thioether functionalized organic–inorganic mesoporous composite as a highly selective and capacious Hg²⁺ adsorbent. *Chem. Commun.* **2**, 210–211 (2003).
43. Sánchez, G. *et al.* Modified mesoporous silica nanoparticles as a reusable, selective chromogenic sensor for mercury(II) recognition. *Dalton Trans.* **42**(18), 6318–6326 (2013).
44. Wang, X. *et al.* Synthesis of poly (2-aminothiazole) for selective removal of Hg(II) in aqueous solutions. *Ind. Eng. Chem. Res.* **55**(17), 4911–4918 (2016).
45. Wang, S., Wei, M. & Huang, Y. Biosorption of multifold toxic heavy metal ions from aqueous water onto food residue eggshell membrane functionalized with ammonium thioglycolate. *J. Agric. Food Chem.* **61**(21), 4988–4996 (2013).
46. Das, R., Giri, S., Muliwa, A. M. & Maity, A. High-performance Hg(II) removal using thiol-functionalized polypyrrole (PPy/MAA) composite and effective catalytic activity of Hg(II)-adsorbed waste material. *ACS Sustain. Chem. Eng.* **5**(9), 7524–7536 (2017).
47. Mostafa, A. G., Abd El-Hamid, A. I. & Akl, M. A. Surfactant-supported organoclay for removal of anionic food dyes in batch and column modes: adsorption characteristics and mechanism study. *Appl. Water Sci.* **13**(8), 163 (2023).
48. Ouachtak, H. *et al.* Highly efficient and fast batch adsorption of orange G dye from polluted water using superb organo-montmorillonite: experimental study and molecular dynamics investigation. *J. Mol. Liq.* **2021**, 335 (2021).
49. Nasrollahpour, A., Moradi, S. M. J. & Moradi, S. E. Dispersive solid phase micro-extraction of mercury(II) from environmental water and vegetable samples with ionic liquid modified graphene oxide nanoparticles. *J. Serbian Chem. Soc.* **82**(5), 551–565 (2017).
50. Kenawy, I. M., Ismail, M. A., Hafez, M. A. H. & Hashem, M. A. Synthesis and characterization of novel ion-imprinted guanyl-modified cellulose for selective extraction of copper ions from geological and municipality sample. *Int. J. Biol. Macromol.* **115**, 625–634. <https://doi.org/10.1016/j.ijbiomac.2018.04.100> (2018).
51. Astrini, N., Anah, L. & Haryadi, H. R. Adsorption of heavy metal ion from aqueous solution by using cellulose based hydrogel composite. In *Macromolecular Symposia* Vol. 353(1), 191–197. <https://doi.org/10.1002/masy.201550326> (2015).
52. Elmehbad, N. Y. & Mohamed, N. A. Designing, preparation and evaluation of the antimicrobial activity of biomaterials based on chitosan modified with silver nanoparticles. *Int. J. Biol. Macromol.* **151**, 92–103 (2020).
53. Sun, Q. *et al.* Covalent organic frameworks as a decorating platform for utilization and affinity enhancement of chelating sites for radionuclide sequestration. *Adv. Mater.* **30**(20), 1705479 (2018).
54. Sun, X., Zhang, J. & You, Y. Enhancement of Cu(II) removal by carbon disulfide modified black wattle tannin gel. *Colloids Surfaces A Physicochem. Eng. Asp.* **608**, 125594 (2021).
55. Cordova, B. M. *et al.* Xanthate-modified alginates for the removal of Pb (II) and Ni(II) from aqueous solutions: A brief analysis of alginate Xanthation. *Int. J. Biol. Macromol.* **179**, 557–566 (2021).
56. Wang, C., Wang, H. & Gu, G. Ultrasound-assisted xanthation of cellulose from lignocellulosic biomass optimized by response surface methodology for Pb (II) sorption. *Carbohydr. Polym.* **182**, 21–28 (2018).
57. French, A. D. Idealized powder diffraction patterns for cellulose polymorphs. *Cellulose* **21**(2), 885–896 (2014).
58. Maunu, S., Liitiä, T., Kauliomäki, S., Hortling, B. O. & Sundquist, J. 13C CPMAS NMR investigations of cellulose polymorphs in different pulps. *Cellulose* **7**, 147–159 (2000).
59. Wang, Y., Xiao, G., Peng, Y., Chen, L. & Fu, S. Effects of cellulose nanofibrils on dialdehyde carboxymethyl cellulose based dual responsive self-healing hydrogel. *Cellulose* **26**, 8813–8827 (2019).
60. Kenawy, I. M., Hafez, M. A. H., Ismail, M. A. & Hashem, M. A. Adsorption of Cu(II), Cd(II), Hg(II), Pb(II) and Zn(II) from aqueous single metal solutions by guanyl-modified cellulose. *Int. J. Biol. Macromol.* **107**, 1538–1549. <https://doi.org/10.1016/j.ijbiomac.2017.10.017> (2018).
61. Moryganov, A. P., Zavadskii, A. E. & Stokozenko, V. G. special features of x-ray analysis of cellulose crystallinity and content in flax fibres. *Fibre Chem.* **49**(6), 382 (2018).
62. Akindoyo, J. O., Pickering, K., Beg, M. D. & Mucalo, M. Combined digestion and bleaching of New Zealand flax/harakeke fibre and its effects on the mechanical, thermal, and dynamic mechanical properties of poly (lactic) acid matrix composites. *Compos. Part A* **164**, 107326 (2023).
63. Kramar, A., Ivanovska, A. & Kostić, M. Regenerated cellulose fiber functionalization by two-step oxidation using sodium periodate and sodium chlorite—Impact on the structure and sorption properties. *Fibers Polym.* **8**, 2177–2186 (2021).
64. Jabli, M. *et al.* Chemical modification of microcrystalline cellulose with polyethyleneimine and hydrazine: Characterization and evaluation of its adsorption power toward anionic dyes. *Int. J. Biol. Macromol.* **229**, 210–223 (2023).
65. Kumari, S., Mankotia, D. & Chauhan, G. S. Crosslinked cellulose dialdehyde for Congo red removal from its aqueous solutions. *J. Environ. Chem. Eng.* **4**(1), 1126–1136 (2016).
66. Li, J., Wan, Y., Li, L., Liang, H. & Wang, J. Preparation and characterization of 2,3-dialdehyde bacterial cellulose for potential biodegradable tissue engineering scaffolds. *Mater. Sci. Eng. C* **29**(5), 1635–1642 (2009).

67. Anirudhan, T. S. & Shainy, F. Effective removal of mercury(II) ions from chlor-alkali industrial wastewater using 2-mercaptobenzamide modified itaconic acid-grafted-magnetite nanocellulose composite. *J. Colloid Interface Sci.* **456**, 22–31 (2015).
68. Anirudhan, T. S., Suchithra, P. S. & Divya, L. Adsorptive potential of 2-mercaptobenzimidazole-immobilized organophilic hydro-talcite for mercury(II) ions from aqueous phase and its kinetic and equilibrium profiles. *Water Air Soil Pollut.* **196**, 127–139 (2009).
69. Anirudhan, T. S. & Rejeena, S. R. Adsorption and hydrolytic activity of trypsin on a carboxylate-functionalized cation exchanger prepared from nanocellulose. *J. Colloid Interface Sci.* **381**(1), 125–136 (2012).
70. Bisla, V., Rattan, G., Singhal, S. & Kaushik, A. Green and novel adsorbent from rice straw extracted cellulose for efficient adsorption of Hg(II) ions in an aqueous medium. *Int. J. Biol. Macromol.* **161**, 194–203 (2020).
71. Arias, F. E. A., Beneduci, A., Chidichimo, F., Furia, E. & Straface, S. Study of the adsorption of mercury(II) on lignocellulosic materials under static and dynamic conditions. *Chemosphere* **180**, 11–23 (2017).
72. Ofomaja, A. E., Naidoo, E. B. & Pholosi, A. Intraparticle diffusion of Cr(VI) through biomass and magnetite coated biomass: A comparative kinetic and diffusion study. *South Afr. J. Chem. Eng.* **32**(1), 39–55. <https://doi.org/10.1016/j.sajce.2020.01.005> (2020).
73. Şenol, Z. M. & Şimşek, S. Insights into effective adsorption of lead ions from aqueous solutions by using chitosan-bentonite composite beads. *J. Polym. Environ.* **30**(9), 3677–3687. <https://doi.org/10.1007/s10924-022-02464-8> (2022).
74. Mudasar, M. *et al.* Simultaneous adsorption of Zn(II) and Hg(II) ions on selective adsorbent of dithizone-immobilized bentonite in the presence of Mg(II) ion. *J. Environ. Chem. Eng.* **8**(4), 104002. <https://doi.org/10.1016/j.jece.2020.104002> (2020).
75. Wang, C. *et al.* Development of mercaptosuccinic anchored MOF through one-step preparation to enhance adsorption capacity and selectivity for Hg(II) and Pb(II). *J. Mol. Liq.* **317**, 113896. <https://doi.org/10.1016/j.molliq.2020.113896> (2020).
76. Velepini, T. & Pillay, K. Sulphur functionalized materials for Hg(II) adsorption: A review. *J. Environ. Chem. Eng.* **7**(5), 103350 (2019).
77. Kumar, A. S. K., Barathi, M., Puvvada, S. & Rajesh, N. Microwave assisted preparation of glycidyl methacrylate grafted cellulose adsorbent for the effective adsorption of mercury from a coal fly ash sample. *J. Environ. Chem. Eng.* **1**(4), 1359–1367 (2013).
78. Fu, Y. *et al.* Functionalized magnetic mesoporous silica/poly (m-aminothiophenol) nanocomposite for Hg(II) rapid uptake and high catalytic activity of spent Hg(II) adsorbent. *Sci. Total Environ.* **691**, 664–674 (2019).
79. Luo, X. *et al.* Novel thymine-functionalized MIL-101 prepared by post-synthesis and enhanced removal of Hg²⁺ from water. *J. Hazard Mater.* **306**, 313–322 (2016).
80. Chakraborty, A., Bhattacharyya, S., Hazra, A., Ghosh, A. C. & Maji, T. K. Post-synthetic metalation in an anionic MOF for efficient catalytic activity and removal of heavy metal ions from aqueous solution. *Chem. Commun.* **52**, 2831–2834 (2016).
81. Shao, Z. *et al.* Modulation of magnetic behavior and Hg²⁺ removal by solvent-assisted linker exchange based on a water-stable 3D MOF. *Chem. Mater.* **30**, 7979–7987 (2018).
82. Al-Ghamdi, Y. O., Alamry, K. A., Hussein, M. A., Marwani, H. M. & Asiri, A. M. Sulfone-modified chitosan as selective adsorbent for the extraction of toxic Hg(II) metal ions. *Adsorpt. Sci. Technol.* **37**(1–2), 139–159 (2019).
83. Benavente, M. Adsorption of metallic ions onto chitosan: Equilibrium and kinetic studies. The following information is correct: M. Benavente, Adsorption of metallic ions onto chitosan: equilibrium and kinetic studies (Licentiate Thesis in Chemical Engineering) Department of Chemical Engineering and Technology, Royal Institute of Technology (KTH), Stockholm, Sweden, 2008, ISBN 978-91-7178-986-0 (ISSN 1654-1081). Kemiteknik (2008).
84. Wang, D., Marin, L. & Cheng, X. Fluorescent chitosan-BODIPY macromolecular chemosensors for detection and removal of Hg(2+) and Fe(3+) ions. *Int. J. Biol. Macromol.* **198**, 194–203 (2022).
85. Li, C., Duan, L. & Cheng, X. Facile method to synthesize fluorescent chitosan hydrogels for selective detection and adsorption of Hg²⁺/Hg⁺. *Carbohydr. Polym.* **288**, 119417 (2022).
86. Norasikin, S., Khairiraihanna, J. & Hanapi, M. Adsorption characteristics of SulfurFunctionalized silica microspheres with respect to the removal of Hg(II) from aqueous solutions. *Ind. Eng. Chem. Res.* **53**, 1225–1233 (2014).
87. Tauanov, Z., Lee, J. & Inglezakis, V. J. Mercury reduction and chemisorption on the surface of synthetic zeolite silver nanocomposites: Equilibrium studies and mechanisms. *J. Mol. Liq.* **305**, 112825 (2020).
88. Attari, M., Bukhari, S. S., Kazemian, H. & Rohani, S. A low-cost adsorbent from coal fly ash for mercury removal from industrial wastewater. *J. Environ. Chem. Eng.* **5**, 391–399. <https://doi.org/10.1016/j.jece.2016.12.014> (2017).
89. Sobhanardakani, S., Jafari, A., Zandipak, R. & Meidanchi, A. Removal of heavy metal (Hg(II) and Cr(VI)) ions from aqueous solutions using Fe₂O₃@SiO₂ thin films as a novel adsorbent. *Process. Saf. Environ. Prot.* **120**, 348–357. <https://doi.org/10.1016/j.psep.2018.10.002> (2018).
90. Asare, E. A., Essumang, D. K., Dodoo, D. K. & Tagoe, S. Utilization of Bacillus thuringiensis MC28 as a biosorbent for mercury in groundwaters from some selected gold mining communities in the Wassu West District of the Western Region of Ghana. *Environ. Nanotechnol. Monit. Manag.* **9**, 95–106. <https://doi.org/10.1016/j.enmm.2017.12.005> (2018).
91. Park, J. H., Wang, J. J., Zhou, B., Mikhael, J. E. R. & DeLaune, R. D. Removing mercury from aqueous solution using sulfurized biochar and associated mechanisms. *Environ. Pollut.* **244**, 627–635. <https://doi.org/10.1016/j.envpol.2018.10.069> (2019).
92. Vali, S. A., Baghdadi, M. & Abdoli, M. A. Immobilization of polyaniline nanoparticles on the polyurethane foam derived from waste materials: A porous reactive fixed-bed medium for removal of mercury from contaminated waters. *J. Environ. Chem. Eng.* **6**, 6612–6622. <https://doi.org/10.1016/j.jece.2018.09.042> (2018).
93. Mora Alvarez, N. M., Pastrana, J. M., Lagos, Y. & Lozada, J. J. Evaluation of mercury (Hg²⁺) adsorption capacity using exhausted coffee waste. *Sustain. Chem. Pharm.* **10**, 60–70. <https://doi.org/10.1016/j.scp.2018.09.004> (2018).
94. Şahan, T., Erol, F. & Yılmaz, Ş. Mercury(II) adsorption by a novel adsorbent mercaptomodified bentonite using ICP-OES and use of response surface methodology for optimization. *Microchem. J.* **138**, 360–368 (2018).

Author contributions

A.G.M.: Methodology, investigation, writing—original draft, review. E.A.G.: Supervision. M.A.A.: Conceptualization, Methodology, Investigation, Writing—original draft, review, Supervision

Funding

Open access funding provided by The Science, Technology & Innovation Funding Authority (STDF) in cooperation with The Egyptian Knowledge Bank (EKB).

Competing interests

The authors declare no competing interests.

Additional information

Correspondence and requests for materials should be addressed to M.A.A.

Reprints and permissions information is available at www.nature.com/reprints.

Publisher's note Springer Nature remains neutral with regard to jurisdictional claims in published maps and institutional affiliations.



Open Access This article is licensed under a Creative Commons Attribution 4.0 International License, which permits use, sharing, adaptation, distribution and reproduction in any medium or format, as long as you give appropriate credit to the original author(s) and the source, provide a link to the Creative Commons licence, and indicate if changes were made. The images or other third party material in this article are included in the article's Creative Commons licence, unless indicated otherwise in a credit line to the material. If material is not included in the article's Creative Commons licence and your intended use is not permitted by statutory regulation or exceeds the permitted use, you will need to obtain permission directly from the copyright holder. To view a copy of this licence, visit <http://creativecommons.org/licenses/by/4.0/>.

© The Author(s) 2023